Molecular Therapy
Original Article

Improved Efficacy in a Fabry Disease Model Using a Systemic mRNA Liver Depot System as Compared to Enzyme Replacement Therapy

Frank DeRosa,[1] Lianne Smith,[1] Yinghua Shen,[2] Yan Huang,[2] Jing Pan,[2] Hongsheng Xie,[2] Barak Yahalom,[3] and Michael W. Heartlein[1]

[1]Translate Bio, Lexington, MA 02141, USA; [2]Shire Pharmaceuticals, Lexington, MA 02141, USA; [3]Biomere, Worcester, MA 01608, USA

Fabry disease is a lysosomal storage disorder caused by the deficiency of α-galactosidase A. Enzyme deficiency results in a progressive decline in renal and cardiac function, leading to cardiomyopathy and end-stage renal disease. Current treatments available, including enzyme replacement therapies, have provided significant benefit to patients; however, unmet medical needs remain. mRNA therapy, with drug-like properties, has the unique ability to produce therapeutic proteins endogenously. Here we describe the sustained delivery of therapeutic human α-galactosidase protein *in vivo* via nanoparticle-formulated mRNA in mouse and non-human primate, with a demonstration of efficacy through clinically relevant biomarker reduction in a mouse Fabry disease model. Multi-component nanoparticles formulated with lipids and lipid-like materials were developed for the delivery of mRNA encoding human α-galactosidase protein. Upon delivery of human GLA mRNA to mice, serum GLA protein levels reached as high as ~1,330-fold over normal physiological values.

INTRODUCTION

Fabry disease is an X-linked lysosomal storage disorder (LSD) that is a result of mutations in the gene (GLA) that encodes the lysosomal enzyme α-galactosidase A.[1–3] Loss of GLA enzyme activity results in improper metabolism of glycolipids containing α-D-galactosyl moieties, such as globotriaosylceramide (Gb3, also known as ceramide trihexoside) and its deacylated metabolite lyso-globotriaosylceramide (lyso-Gb3).[4–6] Accumulation of these fatty lipids is observed within the lysosomes of multiple tissues, including liver, spleen, kidney, and heart, as well as the vasculature and plasma. Progressive accumulation of such lipids leads to clinical disease, manifesting as angiokeratomas, congestive heart failure, stroke, myocardial infarction, and end-stage renal failure ultimately leading to fatality.[2,7–9]

Current therapies approved for the treatment of Fabry disease include enzyme replacement therapies (ERTs)[10,11] and, more recently, a small molecule chaperone (migalastat).[12,13] Two ERT-based treatments are human recombinant forms of α-galactosidase A (agalsidase), known as agalsidase-α (Replagal, Shire, Lexington, MA) and agalsidase-β (Fabrazyme, Sanofi-Genzyme, Cambridge, MA), which are each administered intravenously once every other week and provide beneficial effects toward slowing the progression of the disease.[14–17] While therapeutic value has been demonstrated through this approach, there are challenges associated with ERT and unmet medical needs still remain. Such challenges include variability of response, immunogenicity of the recombinant protein resulting in antibody generation (including neutralizing), infusion reactions, and difficulties inherent with cell-based manufacturing such as robust reproducibility of proper glycosylation patterns.[11,18–26]

An alternative approach to the treatment of Fabry disease is through the application of mRNA therapeutics. Systemic mRNA therapy (MRT) is a recent approach to the delivery of therapeutic proteins *in vivo*, using biosynthetic mRNA transcripts as the source for therapeutic protein.[27–33] Applications of mRNA have recently demonstrated potential therapeutic value in the treatment of various diseases.[34–38] Protein production derived from the exogenous mRNA takes advantage of the endogenous protein translational machinery within the body while incorporating all of the endogenous post-translational modifications through processing pathways that are present in human cells and tissues.[39–42] Such modifications include proper folding, glycosylation, and trafficking within the cell to the target site of action. Directing endogenous production of the deficient enzyme, such as for GLA to restore lysosomal function, to occur within the patient's own body may afford solutions to some of the difficulties faced when using an ERT-based approach.

Exploiting this key feature of MRT could enable the treatment of many diseases, including those in which protein-based therapeutics are not currently possible, such as large transmembrane proteins[43–45] or proteins requiring cytoplasmic delivery.[46–48] Moreover, MRT could provide flexibility with respect to delivery within the body. The ultimate site of mRNA delivery and subsequent translation need not be within the target organ to achieve a therapeutic benefit.[49] In many cases, protein translated from the delivered mRNA is

Received 7 November 2018; accepted 1 March 2019;
https://doi.org/10.1016/j.ymthe.2019.03.001.

Correspondence: Michael W. Heartlein, Translate Bio, 29 Hartwell Avenue, Lexington, MA 02421, USA
E-mail: mheartlein@translate.bio

Please cite this article in press as: DeRosa et al., Improved Efficacy in a Fabry Disease Model Using a Systemic mRNA Liver Depot System as Compared to Enzyme Replacement Therapy, Molecular Therapy (2019), https://doi.org/10.1016/j.ymthe.2019.03.001

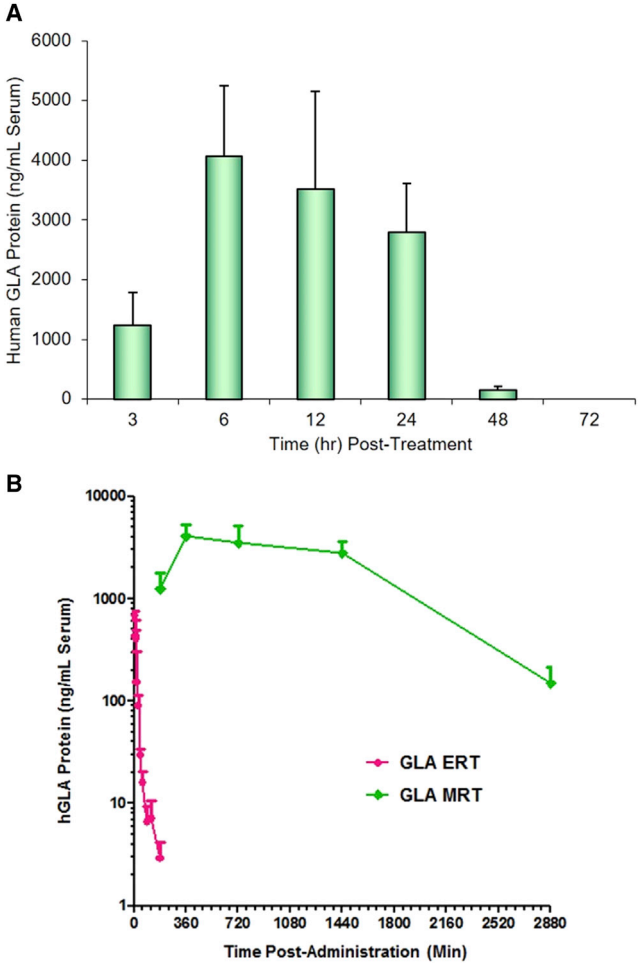

Figure 1. Quantification of Secreted Human α-Galactosidase Protein Levels
(A) Quantification of secreted human α-galactosidase (hGLA) protein levels as measured via ELISA (N = 4 mice per group, error bars represent SD). The protein detected is a result of its production from hGLA mRNA delivered intravenously via a single dose of lipid nanoparticles (1.0 mg/kg encapsulated hGLA mRNA) over time (72 h). Aliquots of mouse serum were collected at the designated time points. (B) Comparison of hGLA protein levels after treatment with either hGLA mRNA LNPs (MRT) or direct injection of hGLA protein (ERT), as measured by ELISA. A prolonged exposure of hGLA protein is achieved when it is derived from hGLA mRNA. Aliquots of mouse serum were collected at the designated time points. All data are mean ± SD.

secreted, as is the case with GLA, to treat the respective disease systemically. Finally, MRT has additional potential advantages over other nucleic acid platforms such as gene therapy, including the lack of requirement for nuclear localization and elimination of insertional mutagenesis risks.

As with most nucleic acid-based therapeutics, intracellular delivery is required to achieve function. mRNA is a transient molecule by nature, and, therefore, efficient delivery requires a vehicle that can protect it from degradation, primarily caused through nuclease activity.[50] The encapsulation of RNA within lipid nanoparticles (LNPs) can also provide for sustained RNA stability.[51] We have previously reported the development of therapeutic mRNA-loaded LNPs,[34] and other publications have explored the optimization of such systems for the specific delivery of mRNA.[52–55] In general, LNPs are formulated with either a cationic or ionizable lipid or lipid-like helper lipids, and a nucleic acid payload. Proper selection of lipid components and design of the LNP can facilitate accumulation in specific sites within the body by manipulation of size and/or inclusion of targeting agents.[56–61]

Here we describe the first example of efficacy in a Fabry disease mouse model using a lipid-based LNP formulation for systemic delivery of mRNA, *in vivo*, derived from our MRT platform. A formulation containing the cationic lipidoid C12-200[62] was developed for the delivery of *in vitro*-synthesized mRNA encoding human α-galactosidase (hGLA) enzyme. Delivery of the mRNA to hepatocytes was confirmed using *in situ* hybridization (ISH) methods, and, subsequently, high levels of hGLA protein production from the exogenously synthesized mRNA transcript were observed and quantified in multiple organs and serum. Favorable pharmacokinetic properties, including dramatically increased area under the curve (AUC), with MRT as compared to ERT were demonstrated, resulting in enhanced biodistribution and deposition of hGLA protein in key organs. Finally, proof of efficacy with GLA MRT was established in a Fabry (GLA^{tm1kul}) mouse model,[63] demonstrating increased GB3 substrate clearance and evidence for improved dosing regimen (monthly versus biweekly) compared to results with ERT.

RESULTS

We examined the potential of LNP-formulated mRNA to produce hGLA therapeutic protein, in both wild-type and diseased mice. Quantitative measurement demonstrated that the desired protein derived from exogenous human mRNA was delivered at supraphysiological levels via LNP formulations. Protein secretion resulted in an extended pharmacokinetic exposure profile as well as enhanced therapeutic efficacy in a knockout (KO) mouse model.

hGLA Protein Production in Wild-Type Mice

To evaluate the ability of mRNA-encapsulated LNPs to facilitate the delivery of mRNA, we monitored both hGLA mRNA and hGLA protein levels in select tissues and serum over 72 h in wild-type mice. This was performed as a single-dose administration (1.0 mg/kg based on encapsulated mRNA) given intravenously. All formulations were well tolerated in the mice at the given dose with no observable adverse events.

Following a single intravenous administration of hGLA mRNA LNPs, high levels of hGLA protein were detected in the sera of treated mice. As early as 3 h post-administration, hGLA protein was present at markedly higher quantities than physiological levels found in normal, healthy mice, yielding a maximum serum concentration at approximately 6 h post-dose. As shown in Figure 1A, upon treatment with a 1.0-mg/kg dose of hGLA mRNA-encapsulated LNPs, approximately 4 μg hGLA protein/mL serum was produced. This is

Please cite this article in press as: DeRosa et al., Improved Efficacy in a Fabry Disease Model Using a Systemic mRNA Liver Depot System as Compared to Enzyme Replacement Therapy, Molecular Therapy (2019), https://doi.org/10.1016/j.ymthe.2019.03.001

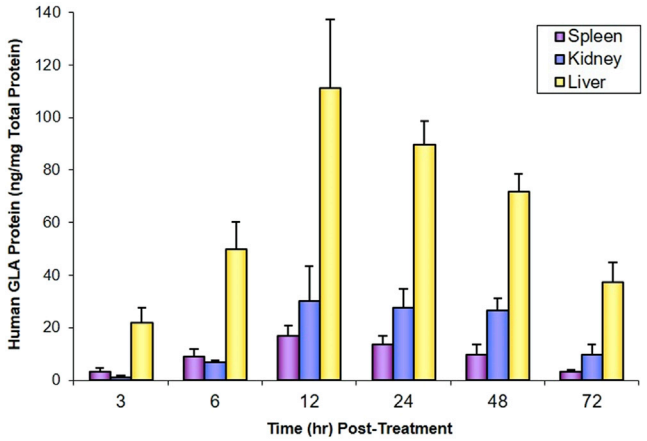

Figure 2. Quantification of hGLA Protein Levels

Quantification of hGLA protein levels in selected organs as measured by ELISA (N = 4 mice per group, error bars represent SD). The protein detected is a result of its production, over a period of 72 h, from hGLA mRNA delivered intravenously via a single dose of lipid nanoparticles (1.0 mg/kg encapsulated hGLA mRNA). Tissues were harvested at the designated time points, homogenized, and analyzed. All data are mean ± SD.

~1,330-fold over the normal human physiological level of GLA (average normal levels reported to be approximately 3.0 ng/mL).[64] Supraphysiological levels of protein (~148 ng/mL) were still observed at 48 h post-administration. These data demonstrate the ability of organs that internalize LNP-delivered mRNA to act as a depot for the production (and secretion) of hGLA protein. Such a phenomenon has been reported previously using mRNA for producing proteins, including hEPO and hFIX proteins.[32,34]

A comparison of the pharmacokinetic profile of serum levels between MRT-derived hGLA protein and direct injection of hGLA ERT was explored. A clear difference was observed when comparing the blood residence times and AUCs for either MRT or ERT (Figure 1B). The reported circulation half-life ($\tau_{1/2}$) of hGLA protein ranges from 42 to 117 min, with an average of approximately 83 min.[65] In the example shown in Figure 1B, the measured $\tau_{1/2}$ of hGLA protein after ERT administration was approximately 16 min. However, hGLA MRT was found to greatly prolong serum half-life. Specifically, after treatment with a 1.0-mg/kg single-dose administration of hGLA mRNA LNPs, we observed a marked increase in the half-life of hGLA protein in the serum, resulting in a value of approximately $\tau_{1/2}$ = 7.5 h. A comparison of the AUCs results in an increase of approximately 17-fold for MRT versus ERT after normalization, respectively. Such a large difference in systemic exposure to hGLA is likely caused by the continuous endogenous production of hGLA protein from the LNP-delivered hGLA mRNA. The biosynthetic mRNA engages the endogenous ribosomal machinery, which continuously translates hGLA protein until the mRNA is expended.

Select organs (liver, spleen, and kidney) were harvested and analyzed to understand the biodistribution, trafficking, and accumulation of hGLA protein upon treatment with hGLA mRNA LNPs. Quantification of hGLA within these organs was achieved using ELISA methods for analysis, with the livers showing the most abundant levels of hGLA protein present (Figure 2). This is not surprising as the C12-200-based LNPs utilized in this experiment have been designed to preferentially accumulate in the liver through passive targeting. Detectable levels were achieved in both the spleen and kidney as well at all time points tested, with the maximum levels for all organs achieved between 12 and 24 h. More specifically, as the kidney is a primary organ affected by Fabry disease, levels within this tissue reached 30 ng hGLA/mg total protein 12 h after administration, representing an order of magnitude increase over normal physiological levels found within the kidney (~2.7 ng/mg total protein).[64]

Enzyme activity analyses were performed to determine if the MRT-derived hGLA protein observed in the serum of treated mice was functional. To achieve this, a fluorescence-based assay was designed based on cleavage of an α-galactose-linked substrate, galactosylated 4-methylumbelliferyl substrate (4-MU-α-gal). Upon cleavage of the sugar moiety, a fluorescent product, 4-methylumbelliferone (4-MU), can be quantitatively measured. Analysis of serum samples of mice after treatment with hGLA mRNA-loaded LNPs resulted in active hGLA with a specific activity range of 2.2–4.4 nmol/h/ng hGLA protein. Similar values were measured for recombinant hGLA protein, which resulted in a specific activity range of 2.1–4.2 nmol/h/ng hGLA protein. These findings confirm the ability of exogenously produced mRNA to successfully produce endogenous active protein within a living system.

Additional studies were performed to further understand the pharmacokinetics of mRNA deposition and subsequent protein production and secretion at earlier time points, in both the liver and kidney after treatment with hGLA mRNA LNPs. Cell-specific uptake and biodistribution were visualized using both ISH and immunohistochemistry (IHC) methods. The LNP system employed in these studies was designed for enrichment to the liver through passive targeting, resulting in successful delivery and deposition of biosynthetic hGLA mRNA as determined using ISH. Detection of hGLA mRNA was achieved with visualization in both hepatocytes as well as other sinusoidal cells within treated mouse livers, as early as 30 min post-administration of hGLA mRNA-loaded LNPs (Figure S1). No cross-reactivity was observed for endogenous mouse GLA transcripts. mRNA was still present at detectable levels within the hepatocytes upon ISH analysis up to 48 h after a single dose.

hGLA protein production, as a result of mRNA treatment, was visualized in the livers and kidneys of the treated mice using IHC methods. Widespread distribution of hGLA protein was observed in both the livers and kidneys of treated mice 24 h after the administrations of hGLA mRNA LNPs, with no cross-reactivity observed in untreated tissue samples (Figure 3). Specifically, hGLA protein was observed in hepatocytes and sinusoidal cells within the livers. Further

Please cite this article in press as: DeRosa et al., Improved Efficacy in a Fabry Disease Model Using a Systemic mRNA Liver Depot System as Compared to Enzyme Replacement Therapy, Molecular Therapy (2019), https://doi.org/10.1016/j.ymthe.2019.03.001

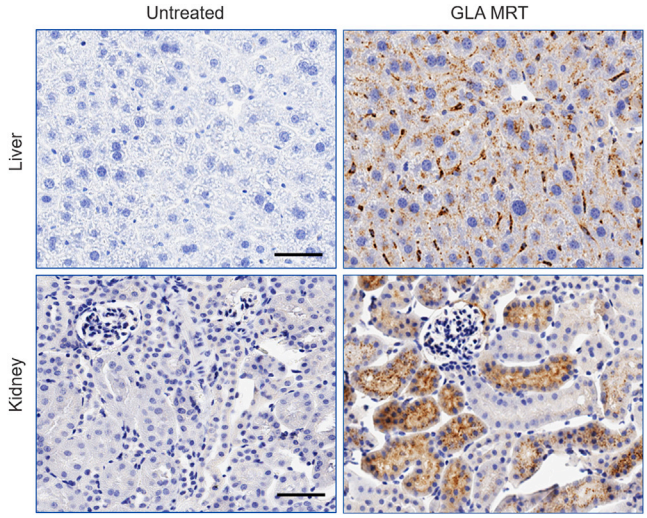

Figure 3. Detection of MRT-Derived Human GLA Protein within Liver and Kidney via Immunohistochemical Staining

Positive staining in livers was observed in hepatocytes as well as sinusoidal cells. Successful detection of hGLA protein in kidneys was also observed. No positive detection of hGLA protein was observed in untreated control tissues. Scale bars, 700 μm (top) and 200 μm (bottom).

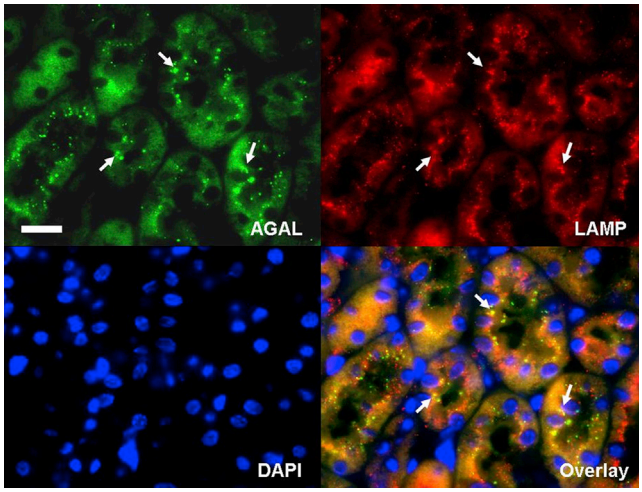

Figure 4. Immunofluorescent Co-localization Studies Performed on Kidneys

Immunofluorescent co-localization studies performed on kidneys of wild-type mice 24 h after treatment with hGLA MRT (1.0 mg/kg). MRT-derived hGLA protein was successfully detected within intracellular vesicles (green). Lysosomal-associated membrane protein LAMP-1 staining was achieved (red). Nuclei of cells were detected via DAPI staining (blue). An overlay of all three staining methods resulted in the successful determination of lysosomal localization of the hGLA protein within the kidneys (yellow). White arrows indicate intracellular vesicles. Scale bar, 50 μm.

IHC analysis of hGLA protein within the livers as a function of time was performed (Figure S2). Although exogenous hGLA mRNA could be visualized at the earliest time point tested (30 min), MRT-derived hGLA protein was weakly observed as early as 2 h post-administration, and it increased over time with maximum staining observed 12–24 h post-administration. These results are consistent with the findings by ELISA. Such an apparent lag in protein production from mRNA deposition can be attributed to the time it takes to engage the endogenous ribosomal machinery and begin to produce hGLA protein to accumulated levels high enough for detection using such methods. Positive staining was observed for up to 72 h after a single dose.

IHC analysis of hGLA protein within the kidneys of treated mice was analyzed over 72 h following a single intravenous dose of hGLA mRNA-loaded LNPs (1.0 mg/kg; Figure S3). Clear detection of hGLA protein was not observed until approximately 12 h post-administration, and detectable levels were still present at 72 h. This discrepancy for timing of detectable hGLA protein levels in liver versus kidney (2 versus 12 h) could be attributed to the origin of hGLA protein observed in the kidney. As these LNPs are designed for preferential delivery to the liver,[34] most of the protein is produced within this organ. Alpha-galactosidase is a secreted protein, and, thus, liver-derived hGLA protein that has been secreted into the bloodstream can circulate and redistribute to other organs, such as the kidney. Supporting data for this natural biological process were found through closer examination of the IHC staining within the kidney (Figure S4). High-magnification images of hGLA staining within the kidney at 12 h post-administration showed the majority of the hGLA residing within the lumen of the proximal tubules. A shift in staining distribution occurred by 24 h, resulting in an increase in punctate, *intracellular* hGLA protein within the tubular epithelial cells with less anti-hGLA staining in the lumen. By 72 h post-administration, we only observed intracellular hGLA protein staining. These results are, therefore, consistent with initial extracellular uptake of hGLA protein from a mechanism involving protein secretion from a peripheral organ (such as the liver). Nevertheless, although these mRNA-loaded LNPs predominantly distributed to the liver, small amounts of hGLA mRNA were detected in the kidneys of treated mice (data not shown). As such, low levels of the detected hGLA protein might have originated from hGLA mRNA directly taken up into the kidney.

The punctate nature of the observed IHC staining of hGLA protein within the kidneys is consistent with this enzyme's primary function within the lysosomes of cells. To establish proper trafficking of MRT-derived hGLA protein, co-localization studies employing fluorescent IHC staining were performed (Figure 4). Human GLA (hGLA)-specific fluorescent staining (green) was achieved and compared with fluorescent detection of the lysosomal-associated membrane protein LAMP-1 (red). Using DAPI as a nuclear stain (blue), co-localization of hGLA protein within the lysosome was visualized (yellow). Deeper immunohistochemical analysis revealed further cellular biodistribution data within the kidney (Figure S5). Detection of hGLA protein within interstitial cells and capillary endothelial cells of the peritubular regions was observed 24 h after treatment of

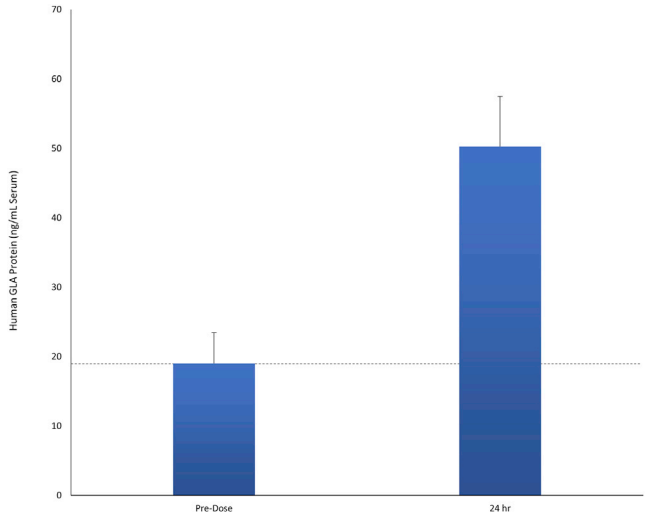

Figure 5. Quantification of Secreted hGLA Protein Levels in Male Marmosets

Quantification of secreted hGLA protein levels in male marmosets as measured via ELISA (N = 2 marmosets, error bars represent SD). The protein detected is a result of its production from hGLA mRNA delivered intravenously via a single dose of lipid nanoparticles (0.10 mg/kg encapsulated hGLA mRNA). The dotted line represents pre-dose background levels due to cross-reactivity with monkey GLA protein. All data are mean ± SD.

hGLA-mRNA LNPs. The presence of hGLA within these cells was observed via IHC for up to 72 h post-administration (data not shown).

hGLA Protein Production in Monkeys

To further evaluate the potential of this formulation in a second species, we dosed male common marmoset monkeys (*Callithrix jacchus*) (2–2.5 years old) with hGLA mRNA LNPs. Each monkey received a single bolus, intravenous injection via the tail vein of human hGLA mRNA LNPs at 0.10 mg/kg dose (two monkeys). A saline flush was administered pre- and post-administration for the LNP-treated monkeys. Serum levels of hGLA protein were monitored pre-dose and 24 h post-administration. Detectable pre-dose levels of hGLA were observed, and they were attributed to some cross-reactivity of the antibodies used due to the high degree of homology between human and primate GLA sequences. After 24 h post-administration, a clear increase in hGLA protein levels was detected in the serum (50 ng hGLA/mL serum) (Figure 5). The formulation was well tolerated by the monkeys with no adverse clinical signs.

In sum, these data clearly demonstrate the ability to effectively deliver mRNA to the liver following the administration of mRNA-loaded LNPs. The exogenous hGLA mRNA was efficiently processed by the host translational machinery to produce a fully formed, functional protein. Further, these results are consistent with a depot effect that provides supraphysiological levels of the desired protein secreted systemically. The hGLA mRNA depot also provides prolonged hGLA plasma exposure profiles as compared to direct injection of ERT with hGLA protein.

hGLA Protein Production and Efficacy in GLA-KO Mouse Disease Model

We sought to demonstrate MRT as an effective therapeutic modality, and, therefore, we applied hGLA mRNA LNPs to an established GLA-KO mouse disease model, GLA^{tm1kul}, which was created through a 1-kb deletion spanning a portion of exon III and intron III within the GLA gene.[63] Production, biodistribution, and efficacy measures were pursued. Efficacy was determined by monitoring the clearance of clinically relevant glycosphingolipid markers known as Gb3 and lyso-Gb3, a known deacylated metabolite of Gb3. These fatty lipid materials accumulate within multiple organs of patients suffering from Fabry disease and lead to detrimental effects, such as cardiomyopathy and renal failure. The mouse disease model utilized in these studies recapitulates the accumulation of Gb3 and lyso-Gb3 in the heart and kidney (among other organs). Both of these lipids can be readily monitored and quantified.

Biodistribution studies involving a direct comparison of hGLA MRT and hGLA ERT modalities in GLA-KO mice were performed. Specifically, GLA-KO mice were treated with a 1.0-mg/kg single intravenous dose of either hGLA mRNA LNPs or hGLA protein, respectively. Serum levels of hGLA protein were monitored at 6 h post-administration for each modality, and selected tissue samples (liver, spleen, kidney, and heart) were harvested 1 week post-administration.

hGLA levels detected in the sera of mice after treatment of GLA-KO mice with either 1.0 mg/kg hGLA MRT or hGLA ERT are provided in Figure S6. As observed in wild-type mice (Figure 1A), supraphysiological levels (4 μg/mL serum) of hGLA protein were observed 6 h post-administration of hGLA mRNA LNPs in these GLA-deficient mice. No hGLA protein was observed in the sera of mice 6 h after direct intravenous injection of hGLA protein ERT. This is not surprising, however, as the blood residence time is markedly shorter, as described earlier, and by 6 h post-administration, all detectable hGLA protein was cleared or taken up into peripheral organs.

Organs were harvested 1 week after a single 1.0-mg/kg treatment with either hGLA MRT or hGLA ERT in the KO mouse model. Specifically, hGLA protein levels were analyzed and quantified in liver, spleen, heart, and kidney using ELISA (Figure S7). hGLA was detected in all tissues tested after both treatments. Specifically, liver hGLA protein levels 1 week after administration were 60 ng hGLA/mg total protein and 49 ng hGLA/mg total protein for MRT and ERT, respectively. Spleen levels measured at 3.8 ng hGLA/mg total protein and 6.9 ng hGLA/mg total protein for MRT versus ERT, respectively. The heart and kidney are typically the source of major complications and pathology in Fabry patients. Comparative analysis of hGLA protein accumulation in the heart 1 week after treatment via MRT or ERT resulted in the accumulation of over 10-fold more hGLA protein upon treatment with MRT (Figure S8). Specifically, protein levels of 11.5 ng hGLA/mg total protein and 1.0 ng hGLA/mg total

Please cite this article in press as: DeRosa et al., Improved Efficacy in a Fabry Disease Model Using a Systemic mRNA Liver Depot System as Compared to Enzyme Replacement Therapy, Molecular Therapy (2019), https://doi.org/10.1016/j.ymthe.2019.03.001

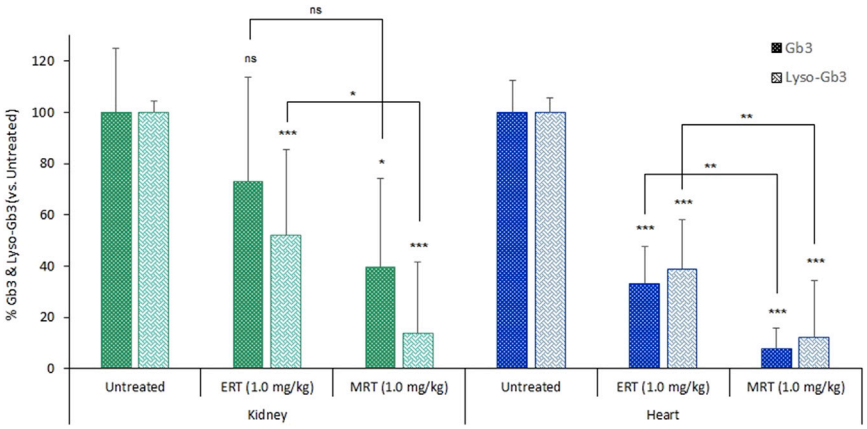

Figure 6. Quantification of Gb3 and lyso-Gb3 Biomarkers in the Kidneys and Hearts of Treated GLA-KO Mice

Levels of Gb3 and lyso-Gb3 were measured 1 week post-administration of either hGLA ERT or hGLA MRT (N = 4 mice per group, error bars represent SD). Enhanced biomarker reduction was observed for treatment with MRT as compared to ERT after a single-dose administration. Data were normalized to untreated mice and represented as a percentage of accumulated levels in untreated kidney and heart. Statistical analysis: ns, not significant; *$p < 0.05$ and ***$p < 0.001$. All data are mean ± SD.

protein were observed for MRT and ERT, respectively. A similar analysis of kidney tissues 1 week after treatment via MRT or ERT resulted in the accumulation of approximately 7-fold more with MRT than with ERT, with levels of 2.42 ng GLA/mg total protein and 0.37 ng GLA/mg total protein, respectively (Figure S8). Such augmented accumulation in the kidneys and heart for MRT-derived hGLA protein may be because of continuous protein production, which resulted in longer blood circulation times (days) and ultimately greater exposure to peripheral organs.

Because MRT-based hGLA protein production had demonstrated favorable properties in relation to both pharmacokinetics and biodistribution, we sought to establish if these effects would translate into superior efficacy when compared with ERT. Therefore, Gb3 and lyso-Gb3 levels were measured in both the kidneys and heart 1 week after a 1.0-mg/kg single-dose administration of either hGLA MRT or hGLA ERT (Figure 6). The ERT approach resulted in decreases in both Gb3 and lyso-Gb3 in the kidney of approximately 27% and 48%, respectively, as compared to normalized levels observed in untreated GLA-KO mice. A more striking significant decrease in kidney Gb3 and lyso-Gb3 levels was observed upon treatment of a 1.0-mg/kg single dose of hGLA mRNA LNPs when using the hGLA MRT approach. Specifically, 66% and 73% clearances of Gb3 and lyso-Gb3 were observed after treatment with hGLA MRT, respectively. Similar trends were observed upon the analysis of biomarker clearance within the hearts of treated GLA-KO mice. For example, significant decreases in Gb3 and lyso-Gb3 of 67% and 61%, respectively, were observed after treatment with hGLA ERT. In contrast, hGLA MRT resulted in more effective clearance, with 92% and 88% decreases in Gb3 and lyso-Gb3 levels, respectively.

Due to this enhancement in biomarker clearance in both the kidneys and heart, we conducted a subsequent study for comparative analysis upon multi-dose regimens. Glycosphingolipid clearance within the kidneys and heart was monitored upon either weekly dosing of hGLA ERT or monthly dosing of hGLA MRT over the course of 2 months. In total, clearance of Gb3 and lyso-Gb3 was monitored after 8 weekly doses of hGLA protein (ERT) or 2 monthly doses of hGLA mRNA LNPs (MRT). The time-elapsed post-final dose equates to 7 days for ERT and 28 days for MRT-based treatment. Key organs were harvested upon completion (day 57) and analyzed accordingly for each biomarker (Figure 7). Equivalent clearance of Gb3 was observed upon analysis of the kidneys, resulting in decreases of 42% and 46% for ERT and MRT, respectively. Kidney levels of lyso-Gb3 were decreased 82% and 69% for ERT and MRT, accordingly. The differences for biomarker clearance in the kidney between the two modalities, ERT and MRT, did not reach statistical significance, representing equivalent reduction for each, even though MRT was dosed only on a monthly regimen. Biomarker clearance within the hearts of the treated KO mice resulted in clearances of Gb3 of 91% and 89% for ERT and MRT, respectively. Further, levels of lyso-Gb3 were lowered by 82% and 64% for ERT and MRT, respectively.

DISCUSSION

We present here the successful application of an mRNA-loaded LNP delivery system directed toward liver (hepatocyte) deposition of hGLA mRNA with subsequent high-level production of hGLA protein in mice and monkeys. We have previously demonstrated the use of LNPs for the successful delivery of mRNA encoding human clotting Factor IX, including subsequent protein production and demonstration of therapeutic benefit in a hemophilia B mouse model.[34] The efficacy observed in that model was achieved through the liver, which served as a depot for secreted production and systemic distribution of therapeutic protein. The present work utilized this inherent feature of an mRNA-based approach to reproducibly express hGLA protein at supraphysiological levels over several days, resulting in favorable pharmacokinetic, biodistribution, and therapeutic properties when compared to an enzyme replacement therapy (ERT) approach.

We provided a biosynthetic hGLA mRNA encapsulated within a LNP as a single dose to wild-type mice, which resulted in high-level hGLA protein production, reaching supraphysiological levels in the serum greater than 1,300-fold over endogenous levels (4 μg/mL).[64] Peak serum concentration was reached within 6 h post-administration

Please cite this article in press as: DeRosa et al., Improved Efficacy in a Fabry Disease Model Using a Systemic mRNA Liver Depot System as Compared to Enzyme Replacement Therapy, Molecular Therapy (2019), https://doi.org/10.1016/j.ymthe.2019.03.001

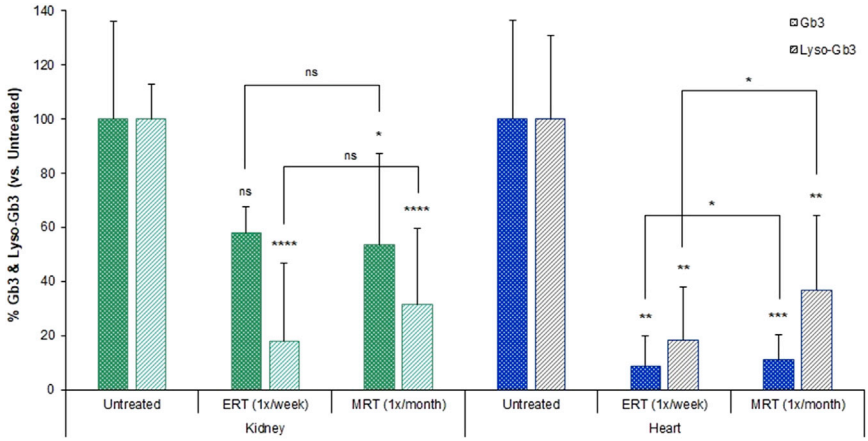

Figure 7. Quantification of Gb3 and lyso-Gb3 Biomarkers in the Kidneys and Hearts of Treated GLA-KO Mice after Multi-dose Regimens for hGLA ERT (Q1W × 8) and hGLA MRT (Q1M × 2)

Levels of Gb3 and lyso-Gb3 were measured 1 week post-final administration of hGLA ERT and 28 days post-final administration of hGLA MRT (N = 5 mice per group, error bars represent SD). Similar biomarker reduction was observed for treatment with monthly MRT dosing as compared to weekly ERT dosing. Data were normalized to untreated mice and represented as a percentage of accumulated levels in untreated kidney and heart. Statistical analysis: ns, not significant; *$p < 0.05$, **$p < 0.01$, ***$p < 0.001$, and ****$p < 0.0001$. All data are mean ± SD.

and was detected for up to 48 h. A pharmacokinetic profile dramatically different from the current standard of care, ERT, was established with MRT (Figure 1B). The reported range of serum half-life of hGLA protein is approximately 42 to 117 min (average 83 min).[65] The blood exposure time was dramatically increased when measuring MRT-derived hGLA protein, resulting in an apparent serum half-life of approximately 7.5 h. We believe this measured half-life incorporates the intrinsic $\tau_{1/2}$ of hGLA protein, which remains constant at what has been previously reported (i.e., 42–117 min). Therefore, the exaggerated blood residence of mRNA-derived hGLA likely results from the continuous translation of hGLA protein from the exogenously delivered hGLA mRNA templates, with this process continuing until the mRNA is expended. The result of this yields an increase in AUC of approximately 17-fold when compared to ERT.

Because of this extended exposure, we observed efficient tissue distribution, with increased accumulation of mRNA-derived hGLA in the liver, spleen, and kidneys (Figure 2). The largest accumulation was observed in the liver within 12 h after administration, and this is not surprising as the liver is the primary organ for LNP distribution and uptake, as we and others have reported previously.[32,34,54,55,62,66] Renal failure is commonly experienced among patients suffering from Fabry disease, and, therefore, improved uptake of hGLA protein into the kidney might have a therapeutic benefit. Upon a single treatment of hGLA MRT (1.0 mg/kg), we observed levels of hGLA in the kidney (30 ng hGLA/mg total protein) approximately 11-fold higher than physiologically normal levels.[64]

Visualization of hepatocellular hGLA mRNA was achieved through ISH. Efficient liver delivery was achieved, and it was detected at the earliest time point tested (30 min; Figure S1). The exogenous hGLA mRNA was present and detectable via ISH through 48 h, although greatly diminished by this time. This is expected, however, as the hGLA mRNA is naturally biodegradable and, therefore, transient by nature. The resulting MRT-derived hGLA protein within selected organs (liver and kidney) was also visualized using IHC. Widespread distribution of hGLA protein was achieved in the liver and kidney of treated mice 24 h after the administration of hGLA mRNA LNPs (Figure 3). With respect to the liver, hepatocytes as well as sinusoidal cells demonstrated successful uptake and/or production of hGLA protein. To gain insight into the pharmacokinetics of MRT-derived hGLA protein production, IHC analysis of both the liver and kidney was monitored up to 72 h post-administration (Figures S2 and S3 for liver and kidney, respectively). The earliest detection of hGLA protein within the liver was at 2 h post-administration, albeit very weakly observed. By 4 h, high levels of hGLA protein could be observed with the greatest intensity observed within 12–24 h, which correlates closely with the quantitative results measured by ELISA. Detectable levels were found throughout the duration of the experiment up to 72 h post-administration.

As discussed above, hGLA is a secreted protein, and, as it enters the bloodstream, it can circulate and distribute to other organs, including the kidneys. Similar to the analysis for the livers, we explored the use of IHC for hGLA-specific detection throughout the course of the experiment to gain insight into both the pharmacokinetic profile of hGLA within the kidney as well as information on its origin (e.g., from circulating hGLA or from mRNA taken up directly; Figure S3). Therefore, IHC analysis was performed on the kidneys beginning 30 min post-administration through 72 h post-dose. While staining was first observed in the liver within 2 h of dosing, significant staining was not detected in the kidneys until 12 h post-administration. These findings are consistent with LNPs predominantly distributing to the liver upon intravenous administration and with the observation that the majority of hGLA mRNA resides within this organ, as detected via ISH. The endogenous ribosomal machinery within the liver can efficiently process the exogenous hGLA mRNA to produce the corresponding protein, serving as a production depot, in which the hGLA protein can be secreted through its natural trafficking pathway. Because of this, we observed strong extracellular staining within the lumen of the proximal tubules (Figure S4, blue arrows) of the kidneys at the first sign of detection (12 h). The staining distribution changed as time progressed such that, at 24 h, more punctate staining, consistent with intracellular protein, was observed. This trend continued

Please cite this article in press as: DeRosa et al., Improved Efficacy in a Fabry Disease Model Using a Systemic mRNA Liver Depot System as Compared to Enzyme Replacement Therapy, Molecular Therapy (2019), https://doi.org/10.1016/j.ymthe.2019.03.001

through the duration of the study, with most of the detectable hGLA protein residing intracellularly within the kidney by 72 h post-administration (Figure S4, red arrows).

Fabry disease is a lysosomal storage disease caused by mutations in the gene that encodes GLA, a lysosomal enzyme. Therefore, for an mRNA-based modality, it is imperative that the mRNA-derived hGLA protein gain access and function within the lysosomes of affected tissues. To determine the cellular uptake and trafficking of MRT-derived hGLA protein in the kidney, we performed fluorescence-based co-localization studies (Figure 4). Direct co-localization was established through visualization of hGLA protein (green fluorescence) and a lysosomal specific marker known as LAMP-1 (red fluorescence), which upon overlap results in the yellow fluorescent representation as demonstrated in Figure 4. Such findings demonstrate that hGLA protein produced from exogenous hGLA mRNA can result in properly folded, active enzyme, which can distribute and localize properly to lysosomes. We further explored IHC staining of the kidney at high magnification (60×) to confirm which cell types were able to internalize hGLA protein. Figure S5 shows successful detection of hGLA protein within both capillary endothelial cells of the peritubular region and interstitial cells 24 h after treatment with hGLA MRT. Staining within these cells was observed for 72 h post-administration (data not shown). These results demonstrate that MRT-derived hGLA protein can successfully reach the target vesicles (lysosome) of the target cells (epithelial, endothelial, and interstitial) within the target organ (kidney).

Prior to exploring efficacy studies, we sought to confirm our ability to produce hGLA protein after the administration of hGLA mRNA LNPs and further demonstrate its potential in a second species. We chose marmosets for this purpose, and we dosed them through slow intravenous administration at 0.10 mg/kg. The hGLA mRNA LNP was well tolerated, and hGLA protein production was achieved as determined through increased levels of hGLA protein detected in the serum. Specifically, we observed approximately 50 ng hGLA/mL 24 h post-administration (Figure 5). Due to some cross-reactivity between the antibodies employed for the ELISA, some lower level background signal was observed in serum samples pre-dose. Subtracting out this value (19 ng/mL) results in approximately 31 ng hGLA/mL production in these monkeys, which equates to an approximate 10-fold increase over endogenous levels.

Efficacy studies were performed in a GLA-KO (GLA^{tm1kul}) mouse model.[63] We were interested in gaining insight into the production, pharmacokinetics, biodistribution, and biomarker clearance properties of MRT-derived hGLA protein, in addition to comparing mRNA technology to directly administered hGLA enzyme. Therefore, we dosed GLA-KO mice with either a 1.0-mg/kg intravenous administration of hGLA MRT or hGLA ERT, and we analyzed serum levels of hGLA protein at 6 h and selected organ levels of hGLA protein 1 week post-administration.

Supraphysiological hGLA protein levels (4 μg hGLA/mL serum) were measured in the sera of KO mice after treatment with hGLA MRT 6 h post-administration and compared to wild-type mice (Figure S6). As a direct comparison, a dose of 1.0 mg/kg hGLA ERT yielded negligible levels observed at this time point. Due to the characteristic fast clearance of hGLA protein from blood circulation, we expected to observe such levels 6 h post-dose, as the intravenously delivered hGLA protein was cleared to the peripheral organs (liver, spleen, kidney, heart, etc.). We attribute these findings to the unique and advantageous depot effect of MRT, which provides a continuous source of hGLA protein through multiple rounds of translation of the exogenous hGLA mRNA. The extended exposure profile of hGLA MRT resulted in an increased accumulation of hGLA protein within key organs, the heart and kidney, in comparison to hGLA ERT (Figure S8). Upon discovery of this increased accumulation of hGLA, we proposed that a therapeutic advantage could be achieved for hGLA MRT over ERT.

Use of the GLA-KO mouse model provided biomarkers that could be regularly monitored and quantified. Two clinically relevant biomarkers present within this model are the glycosphingolipids known as Gb3 and lyso-Gb3, and they have been shown to accumulate within a variety of tissues among patients with Fabry disease.[4–9] Specifically, accumulation of these biomarkers due to a loss of function of the hGLA enzyme within the heart and kidneys results in symptoms such as diastolic dysfunction and exertional anginal pectoris as well as severely impaired glomerular filtration rates, ultimately leading to cardiomyopathies and end-stage renal disease, respectively. Due to the greatly increased exposure and accumulation of hGLA protein with hGLA mRNA treatment as compared to hGLA ERT, we hypothesized that such favorable pharmacokinetic properties would result in enhanced efficacy. Therefore, biomarker levels were measured in both the kidneys and hearts of KO mice treated with either hGLA MRT versus ERT after single-dose administration of each treatment.

The objective of these treatments is to clear accumulated hGLA substrates from the kidney, heart, and other tissues. As expected, we found that treatment with hGLA ERT resulted in decreases of Gb3 and lyso-Gb3 in the kidney. However, a much greater reduction of both fatty lipids was observed upon treatment with hGLA MRT, resulting in a clearance of 66% and 73% for Gb3 and lyso-Gb3, respectively. Similar effects were also seen for biomarker clearance within the hearts of treated KO mice. A significant decrease in glycosphingolipids was measured after treatment with hGLA ERT, but again clearance was increased with hGLA MRT, resulting in the striking 92% and 88% decreases in Gb3 and lyso-Gb3 levels, respectively. We attribute these findings to the increased levels of hGLA protein that accumulated within these key organs upon treatment using our MRT approach.

Finally, because hGLA MRT provided superior clearance of Gb3 and lyso-Gb3 when compared to equivalent dosing of hGLA ERT, we postulated that a more favorable dosing regimen could provide suitable therapeutic benefit. Currently, approved ERT drugs Fabrazyme and Replagal are dosed once every other week (Q2W) by intravenous administration (1.0 mg/kg and 0.20 mg/kg, respectively). We challenged the potential of MRT by performing a multi-dose,

Please cite this article in press as: DeRosa et al., Improved Efficacy in a Fabry Disease Model Using a Systemic mRNA Liver Depot System as Compared to Enzyme Replacement Therapy, Molecular Therapy (2019), https://doi.org/10.1016/j.ymthe.2019.03.001

head-to-head study comparing hGLA ERT dosed once every week (Q1W) to hGLA MRT dosed once every month (Q1M). After 8 weekly doses of hGLA ERT, decreases of Gb3 and lyso-Gb3 within the kidneys and heart were measured (Figure 7). Very similar decreases were observed after two monthly doses of hGLA MRT. No statistical significance was achieved between ERT and MRT for clearance within these organs, indicating equivalent efficacy for MRT with monthly dosing. These results taken together provide evidence and establish therapeutic potential relevant for enabling an improved treatment for Fabry disease and other lysosomal storage diseases using our MRT approach.

Conclusions

The results presented here clearly demonstrate the power of using MRT, with enhanced pharmacodynamic effects resulting from prolonged hGLA protein production and subsequent secretion for an extended duration. This extended pharmacokinetic profile is a direct result of the depot effect that hGLA mRNA LNPs can provide upon delivery of the mRNA payload. Such an effect can provide therapeutic value to peripheral organs, which benefit from such prolonged exposure. All these characteristics taken together helped to establish superior biomarker reduction with MRT after a single dose, while also demonstrating equivalent efficacy between monthly dosed mRNA and weekly dosed ERT. Such a longer duration of action and, ultimately, longer dosing interval could be of therapeutic value to patients with Fabry disease.

MATERIALS AND METHODS

All animal studies were conducted in accordance with the approval of the local Institutional Animal Care and Use Committee (IACUC).

Lipid Materials

The formulations described herein consisted of multi-component lipid mixtures of specific ratios employing a combination of lipid-like, helper lipids, and PEGylated lipids designed to encapsulate mRNA therapeutic molecules. C12-200 was synthesized as previously described.[62] DOPE (1,2-dioleyl-sn-glycero-3-phosphoethanolamine; Avanti Polar Lipids, AL, USA) and cholesterol (Sigma, MO, USA) served as helper lipids for the nanoparticle. The PEGylated lipid selected was a dimyristoyl glycerol-polyethylene glycol analog with a polyethylene glycol (PEG) molecular weight of approximately 2,000 Da (DMG-PEG-2K), purchased from NOF (Tokyo, Japan).

mRNA Material

hGLA mRNA was synthesized by *in vitro* transcription via T7 RNA polymerase from a plasmid DNA template encoding the gene using unmodified nucleotides, which was followed by the addition of a 5′ cap structure (Cap 1) and a 3′ poly(A) tail of approximately 200 nt in length as determined by gel electrophoresis.[67] Fixed 5′ and 3′ UTRs were constructed to flank the coding sequences of the mRNA.

Formulation Protocol

Representative Example

Aliquots of 50 mg/mL ethanolic solutions of C12-200, DOPE, cholesterol, and DMG-PEG-2K (40:30:25:5 molar ratio, respectively) were mixed and diluted with ethanol to a 3-mL final volume. Separately, an aqueous buffered solution (10 mM citrate/150 mM NaCl [pH 4.5]) of hGLA mRNA was prepared from a 1-mg/mL stock. The lipid solution was injected rapidly into the aqueous mRNA solution (12 mL) and shaken to yield a final suspension in 20% ethanol. The resulting nanoparticle suspension was filtered, diafiltrated with 1× PBS (pH 7.4), concentrated, and stored at 2°C–8°C (final concentration = 0.15 mg/mL GLA mRNA [encapsulated]; % encapsulation = 81%; % recovery = 85%; Z_{ave} = 73 nm [$Dv_{(50)}$ = 56 nm]).

Animal Models

Pharmacokinetic and biodistribution studies used male mice (CD-1), 6 to 8 weeks old. For efficacy experiments, male and female GLA-KO mice (GLA^{tm1kul}, 10–26 weeks old) were used. GLA^{tm1kul}-KO mice were derived through a 1-kb deletion spanning a portion of exon III and intron III.[63] Breeding pairs of these mice were acquired from Jackson Laboratories (Bar Harbor, ME). Male marmoset monkeys (*Callithrix jacchus*) utilized in pharmacodynamic studies were 2–2.5 years old.

Analysis of Protein Produced via Intravenously Delivered mRNA-Loaded Nanoparticles

Injection Protocol

Samples were administered to mice by a single bolus tail vein injection of the specified dose of encapsulated hGLA mRNA-loaded LNPs. Mice were sacrificed and perfused with saline at the designated time points. Male marmosets (*Callithrix jacchus*) were treated with a single intravenous injection with a pre- and post-injection saline flush of a total dose volume of 1 mL via the tail vein.

Isolation of Organ Tissues for Analysis

The organs of each mouse were harvested and stored either in 10% neutral buffered formalin or snap-frozen and stored at −80°C for analysis.

Isolation of Plasma or Serum for Analysis

All animals were euthanized by CO_2 asphyxiation at respective time points post-administration (±5%), followed by thoracotomy and terminal cardiac blood collection. Whole blood (maximal obtainable volume) was collected via cardiac puncture on euthanized animals. For serum collection, whole blood was placed into serum separator tubes, allowed to clot at room temperature for at least 30 min, centrifuged at 22°C ± 5°C at 9,300 × *g* for 10 min, and extracted. For plasma collection, whole blood was placed into either lithium heparin tubes or citrate-coated tubes and processed to plasma. For interim blood collections, approximately 40–50 μL whole blood was collected via facial vein puncture or tail snip. Samples collected from non-treatment animals were used as a baseline level for comparison to study animals.

ELISA Analysis

Quantification of hGLA protein was performed using custom antibodies specific to hGLA protein. Briefly, a capture antibody was mixed with coating buffer (50 mM $NaHCO_3$ [pH 9.6]), placed on a

96-well plate, and incubated at 37°C. Positive control (recombinant hGLA protein) and biological samples were added and incubated further, followed by the addition of a detection antibody and horseradish peroxidase (HRP)-based chromophore generation. Detection was monitored via absorption (450 nm) on a Molecular Device Flex Station instrument.

α-Galactosidase Activity Assay

Enzymatic activity of hGLA protein was determined through quantitative fluorophore generation. Specifically, hGLA activity was determined through the cleavage of a 4-MU-α-gal resulting in 4-MU. Briefly, biological samples (serum and tissues) were incubated with 4-MU-α-gal substrate diluted in reaction buffer for a pre-determined period of time. Upon quenching, the resultant 4-MU was measured via excitation at 360 nm and measurement of its fluorescence at 465-nm wavelength. One unit of activity was reported as the conversion of 1 nmol 4-MU-α-gal to 4-MU in 1 h at 37°C.

hGLA ISH Assay

The detection of exogenous hGLA mRNA was performed using custom, sequence-specific probes developed with proprietary technology (Advanced Cell Diagnostics, Hayward, CA), involving a probe design strategy that allows simultaneous signal amplification and background suppression to achieve single-molecule visualization while preserving tissue morphology. Tissues and cells mounted on slides were first pretreated (antigen retrieval) to prepare for hybridization. Oligonucleotide target probes (up to 20 probe pairs) were hybridized to the RNA in the sample, followed by a series of steps and washes designed to amplify the signal.

hGLA IHC Assay

IHC was performed using a custom protocol developed for the detection of human hGLA protein. Briefly, formalin-fixed paraffin-embedded (FFPE) tissue samples were de-paraffinized and rehydrated. Antigen retrieval was performed prior to immunohistochemical analysis. Specific detection of human hGLA protein was achieved using a human-specific anti-GLA rabbit polyclonal antibody (TK-8, Shire, Lexington, MA). Visualization under light microscopy was achieved following incubation with a biotinylated goat anti-rabbit immunoglobulin G (IgG) secondary antibody and avidin biotin complex (ABC)-HRP for subsequent reaction with 3,3′-diaminobenzidene (DAB) substrate, resulting in the deposition of brown stain. The images were captured using an Aperio ScanScope whole slide scanner.

Gb3 and lyso-Gb3 Isolation and Quantification Assay

Gb3 and lyso-Gb3 levels were analyzed in selected tissues using liquid chromatography-tandem mass spectrometry (LC-MS/MS)-based methods. Selected tissue samples were homogenized, mixed with methanol, and extracted with a chloroform:methanol mixture (2:1). The resulting tissue extracts were placed in a 96-well format and analyzed for the desired biomarker. Specifically, 20 μL extracted supernatant was injected into the LC-MS/MS system and separated using a Phenomenex Mercury Luna C8 column against an acetonitrile-formic acid-methanol gradient. Quantification of Gb3 and lyso-Gb3 was achieved through analyte peak integration as compared to standard curves of each respective biomarker.

SUPPLEMENTAL INFORMATION

Supplemental Information can be found with this article online at https://doi.org/10.1016/j.ymthe.2019.03.001.

AUTHOR CONTRIBUTIONS

L.S. performed all protein quantification studies. F.D. designed and formulated LNP drug products. L.S., F.D., M.W.H., and B.Y. contributed to *in vivo* study designs. B.Y. directed *in vivo* studies. Y.S. performed all biomarker analysis. J.P. was responsible for all histological evaluation and analysis. H.X. contributed to pharmacokinetic analysis.

CONFLICTS OF INTEREST

F.D., L.S., and M.W.H. are employees and shareholders of Translate Bio.

ACKNOWLEDGMENTS

The authors would like to thank Kari Harbert for her work on breeding the GLA- (GLA^{tm1kul}) knockout mouse colony and Kelly Daly for dose administration on all mouse studies. We thank Andrea Clarke for hGLA activity assay work and Lei Cheng for *in situ* hybridization analysis. The authors would like to acknowledge Brad Guild (Shire Pharmaceuticals), who is now deceased, for his contributions to the research presented in this manuscript.

REFERENCES

1. Motabar, O., Sidransky, E., Goldin, E., and Zheng, W. (2010). Fabry disease - current treatment and new drug development. Curr. Chem. Genomics *4*, 50–56.
2. Kubo, T. (2017). Fabry disease and its cardiac involvement. J. Gen. Fam. Med. *18*, 225–229.
3. Schiffmann, R., Hughes, D.A., Linthorst, G.E., Ortiz, A., Svarstad, E., Warnock, D.G., West, M.L., and Wanner, C.; Conference Participants (2017). Screening, diagnosis, and management of patients with Fabry disease: conclusions from a "Kidney Disease: Improving Global Outcomes" (KDIGO) Controversies Conference. Kidney Int. *91*, 284–293.
4. Auray-Blais, C., and Boutin, M. (2012). Novel gb(3) isoforms detected in urine of fabry disease patients: a metabolomic study. Curr. Med. Chem. *19*, 3241–3252.
5. Nowak, A., Mechtler, T.P., Desnick, R.J., and Kasper, D.C. (2017). Plasma LysoGb3: A useful biomarker for the diagnosis and treatment of Fabry disease heterozygotes. Mol. Genet. Metab. *120*, 57–61.
6. Beirão, I., Cabrita, A., Torres, M., Silva, F., Aguiar, P., Laranjeira, F., and Gomes, A.M. (2017). Biomarkers and Imaging Findings of Anderson-Fabry Disease-What We Know Now. Diseases *5*, 15.
7. O'Mahony, C., and Elliott, P. (2010). Anderson-Fabry disease and the heart. Prog. Cardiovasc. Dis. *52*, 326–335.
8. Alroy, J., Sabnis, S., and Kopp, J.B. (2002). Renal pathology in Fabry disease. J. Am. Soc. Nephrol. *13* (*Suppl 2*), S134–S138.
9. Torra, R. (2008). Renal manifestations in Fabry disease and therapeutic options. Kidney Int. Suppl. *74*, S29–S32.
10. Sanchez-Nino, M.D., and Ortiz, A. (2016). Enzyme Replacement Therapy for Fabry Disease. J. Inborn Errors Metab. Screen. *4*, 1–7.
11. Oder, D., Nordbeck, P., and Wanner, C. (2016). Long Term Treatment with Enzyme Replacement Therapy in Patients with Fabry Disease. Nephron *134*, 30–36.

12. Young-Gqamana, B., Brignol, N., Chang, H.-H., Khanna, R., Soska, R., Fuller, M., Sitaraman, S.A., Germain, D.P., Giugliani, R., Hughes, D.A., et al. (2013). Migalastat HCl reduces globotriaosylsphingosine (lyso-Gb3) in Fabry transgenic mice and in the plasma of Fabry patients. PLoS ONE *8*, e57631.

13. Germain, D.P., Hughes, D.A., Nicholls, K., Bichet, D.G., Giugliani, R., Wilcox, W.R., Feliciani, C., Shankar, S.P., Ezgu, F., Amartino, H., et al. (2016). Treatment of Fabry's Disease with the Pharmacologic Chaperone Migalastat. N. Engl. J. Med. *375*, 545–555.

14. Pastores, G.M. (2007). Agalsidase alfa (Replagal) in the treatment of Anderson-Fabry disease. Biologics *1*, 291–300.

15. Lipinski, S.E., Komlodi-Pasztor, E., and Goker-Alpan, O. (2014). Agalsidase Alfa for the Treatment of Fabry Disease: A Closer Look. Clin. Investig. *4*, 567–584.

16. Keating, G.M., and Simpson, D. (2007). Agalsidase Beta: a review of its use in the management of Fabry disease. Drugs *67*, 435–455.

17. Pisani, A., Riccio, E., and Sabbatini, M. (2015). Agalsidase alfa and agalsidase beta in the treatment of Fabry disease: does the dose really matter? Genet. Med. *17*, 21–23.

18. Linthorst, G.E., Hollak, C.E.M., Donker-Koopman, W.E., Strijland, A., and Aerts, J.M. (2004). Enzyme therapy for Fabry disease: neutralizing antibodies toward agalsidase alpha and beta. Kidney Int. *66*, 1589–1595.

19. Mauhin, W., Lidove, O., Masat, E., Mingozzi, F., Mariampillai, K., Ziza, J.M., and Benveniste, O. (2015). Innate and Adaptive Immune Response in Fabry Disease. JIMD Rep. *22*, 1–10.

20. Nicholls, K., Bleasel, K., and Becker, G. (2012). Severe infusion reactions to fabry enzyme replacement therapy: rechallenge after tracheostomy. JIMD Rep. *5*, 109–112.

21. Ghali, J., Nicholls, K., Denaro, C., Sillence, D., Chapman, I., Goldblatt, J., Thomas, M., and Fletcher, J.; Australian State Fabry Disease Treatment Centres (2012). Effect of reduced agalsidase Beta dosage in fabry patients: the Australian experience. JIMD Rep. *3*, 33–43.

22. Smid, B.E., Rombach, S.M., Aerts, J.M.F.G., Kuiper, S., Mirzaian, M., Overkleeft, H.S., Poorthuis, B.J., Hollak, C.E., Groener, J.E., and Linthorst, G.E. (2011). Consequences of a global enzyme shortage of agalsidase beta in adult Dutch Fabry patients. Orphanet J. Rare Dis. *6*, 69–78.

23. Linthorst, G.E., Germain, D.P., Hollak, C.E., Hughes, D., Rolfs, A., Wanner, C., and Mehta, A.; European Medicines Agency (2011). Expert opinion on temporary treatment recommendations for Fabry disease during the shortage of enzyme replacement therapy (ERT). Mol. Genet. Metab. *102*, 99–102.

24. Mehta, A.B. (2013). Fabry disease: is there a role for enzyme replacement therapy? J. Intern. Med. *274*, 329–330.

25. Jenkins, N., Parekh, R.B., and James, D.C. (1996). Getting the glycosylation right: implications for the biotechnology industry. Nat. Biotechnol. *14*, 975–981.

26. Goochee, C.F. (1992). Bioprocess factors affecting glycoprotein oligosaccharide structure. Dev. Biol. Stand. *76*, 95–104.

27. Kormann, M.S.D., Hasenpusch, G., Aneja, M.K., Nica, G., Flemmer, A.W., Herber-Jonat, S., Huppmann, M., Mays, L.E., Illenyi, M., Schams, A., et al. (2011). Expression of therapeutic proteins after delivery of chemically modified mRNA in mice. Nat. Biotechnol. *29*, 154–157.

28. Karikó, K., Muramatsu, H., Keller, J.M., and Weissman, D. (2012). Increased erythropoiesis in mice injected with submicrogram quantities of pseudouridine-containing mRNA encoding erythropoietin. Mol. Ther. *20*, 948–953.

29. Mays, L.E., Ammon-Treiber, S., Mothes, B., Alkhaled, M., Rottenberger, J., Müller-Hermelink, E.S., Grimm, M., Mezger, M., Beer-Hammer, S., von Stebut, E., et al. (2013). Modified Foxp3 mRNA protects against asthma through an IL-10-dependent mechanism. J. Clin. Invest. *123*, 1216–1228.

30. Zangi, L., Lui, K.O., von Gise, A., Ma, Q., Ebina, W., Ptaszek, L.M., Später, D., Xu, H., Tabebordbar, M., Gorbatov, R., et al. (2013). Modified mRNA directs the fate of heart progenitor cells and induces vascular regeneration after myocardial infarction. Nat. Biotechnol. *31*, 898–907.

31. Schrom, E., Huber, M., Aneja, M., Dohmen, C., Emrich, D., Geiger, J., Hasenpusch, G., Herrmann-Janson, A., Kretzschmann, V., Mykhailyk, O., et al. (2017). Translation of Angiotensin-Converting Enzyme 2 upon Liver- and Lung-Targeted Delivery of Optimized Chemically Modified mRNA. Mol. Ther. Nucleic Acids *7*, 350–365.

32. Li, B., Luo, X., Deng, B., Wang, J., McComb, D.W., Shi, Y., Gaensler, K.M., Tan, X., Dunn, A.L., Kerlin, B.A., and Dong, Y. (2015). An Orthogonal Array Optimization of Lipid-like Nanoparticles for mRNA Delivery in Vivo. Nano Lett. *15*, 8099–8107.

33. Wang, Y., Su, H.-H., Yang, Y., Hu, Y., Zhang, L., Blancafort, P., and Huang, L. (2013). Systemic delivery of modified mRNA encoding herpes simplex virus 1 thymidine kinase for targeted cancer gene therapy. Mol. Ther. *21*, 358–367.

34. DeRosa, F., Guild, B., Karve, S., Smith, L., Love, K., Dorkin, J.R., Kauffman, K.J., Zhang, J., Yahalom, B., Anderson, D.G., and Heartlein, M.W. (2016). Therapeutic efficacy in a hemophilia B model using a biosynthetic mRNA liver depot system. Gene Ther. *23*, 699–707.

35. Badieyan, Z.S., Berezhanskyy, T., Utzinger, M., Aneja, M.K., Emrich, D., Erben, R., Schüler, C., Altpeter, P., Ferizi, M., Hasenpusch, G., et al. (2016). Transcript-activated collagen matrix as sustained mRNA delivery system for bone regeneration. J. Control. Release *239*, 137–148.

36. Alberer, M., Gnad-Vogt, U., Hong, H.S., Mehr, K.T., Backert, L., Finak, G., Gottardo, R., Bica, M.A., Garofano, A., Koch, S.D., et al. (2017). Safety and immunogenicity of a mRNA rabies vaccine in healthy adults: an open-label, non-randomised, prospective, first-in-human phase 1 clinical trial. Lancet *390*, 1511–1520.

37. Stadler, C.R., Bähr-Mahmud, H., Celik, L., Hebich, B., Roth, A.S., Roth, R.P., Karikó, K., Türeci, Ö., and Sahin, U. (2017). Elimination of large tumors in mice by mRNA-encoded bispecific antibodies. Nat. Med. *23*, 815–817.

38. Pardi, N., Secreto, A.J., Shan, X., Debonera, F., Glover, J., Yi, Y., Muramatsu, H., Ni, H., Mui, B.L., Tam, Y.K., et al. (2017). Administration of nucleoside-modified mRNA encoding broadly neutralizing antibody protects humanized mice from HIV-1 challenge. Nat. Commun. *8*, 14630.

39. Nabhan, J.F., Wood, K.M., Rao, V.P., Morin, J., Bhamidipaty, S., LaBranche, T.P., Gooch, R.L., Bozal, F., Bulawa, C.E., and Guild, B.C. (2016). Intrathecal delivery of frataxin mRNA encapsulated in lipid nanoparticles to dorsal root ganglia as a potential therapeutic for Friedreich's ataxia. Sci. Rep. *6*, 20019.

40. Antony, J.S., Dewerth, A., Haque, A., Handgretinger, R., and Kormann, M.S.D. (2015). Modified mRNA as a new therapeutic option for pediatric respiratory diseases and hemoglobinopathies. Mol. Cell Pediatr. *2*, 11.

41. Tiwari, P.M., Vanover, D., Lindsay, K.E., Bawage, S.S., Kirschman, J.L., Bhosle, S., Lifland, A.W., Zurla, C., and Santangelo, P.J. (2018). Engineered mRNA-expressed antibodies prevent respiratory syncytial virus infection. Nat. Commun. *9*, 3999–4014.

42. Groth, K., Berezhanskyy, T., Aneja, M.K., Geiger, J., Schweizer, M., Maucksch, L., Pasewald, T., Brill, T., Tigani, B., Weber, E., et al. (2017). Tendon healing induced by chemically modified mRNAs. Eur. Cell. Mater. *33*, 294–307.

43. Roseman, D.S., Khan, T., Rajas, F., Jun, L.S., Asrani, K.H., Isaacs, C., Farelli, J.D., and Subramanian, R.R. (2018). G6PC mRNA Therapy Positively Regulates Fasting Blood Glucose and Decreases Liver Abnormalities in a Mouse Model of Glycogen Storage Disease 1a. Mol. Ther. *26*, 814–821.

44. Bangel-Ruland, N., Tomczak, K., Fernández Fernández, E., Leier, G., Leciejewski, B., Rudolph, C., Rosenecker, J., and Weber, W.M. (2013). Cystic fibrosis transmembrane conductance regulator-mRNA delivery: a novel alternative for cystic fibrosis gene therapy. J. Gene Med. *15*, 414–426.

45. Robinson, E., MacDonald, K.D., Slaughter, K., McKinney, M., Patel, S., Sun, C., and Sahay, G. (2018). Lipid Nanoparticle-Delivered Chemically Modified mRNA Restores Chloride Secretion in Cystic Fibrosis. Mol. Ther. *26*, 2034–2046.

46. Asrani, K.H., Cheng, L., Cheng, C.J., and Subramanian, R.R. (2018). Arginase I mRNA therapy - a novel approach to rescue arginase 1 enzyme deficiency. RNA Biol. *15*, 914–922.

47. An, D., Schneller, J.L., Frassetto, A., Liang, S., Zhu, X., Park, J.S., Theisen, M., Hong, S.J., Zhou, J., Rajendran, R., et al. (2017). Systemic Messenger RNA Therapy as a Treatment for Methylmalonic Acidemia. Cell Rep. *21*, 3548–3558.

48. Jiang, L., Berraondo, P., Jericó, D., Guey, L.T., Sampedro, A., Frassetto, A., Benenato, K.E., Burke, K., Santamaría, E., Alegre, M., et al. (2018). Systemic messenger RNA as an etiological treatment for acute intermittent porphyria. Nat. Med. *24*, 1899–1909.

49. Connolly, B., Isaacs, C., Cheng, L., Asrani, K.H., and Subramanian, R.R. (2018). SERPINA1 mRNA as a Treatment for Alpha-1 Antitrypsin Deficiency. J. Nucleic Acids *2018*, 8247935.

50. Houseley, J., and Tollervey, D. (2009). The many pathways of RNA degradation. Cell *136*, 763–776.

51. Tsui, N.B.Y., Ng, E.K.O., and Lo, Y.M.D. (2002). Stability of endogenous and added RNA in blood specimens, serum, and plasma. Clin. Chem. *48*, 1647–1653.

52. Kauffman, K.J., Dorkin, J.R., Yang, J.H., Heartlein, M.W., DeRosa, F., Mir, F.F., Fenton, O.S., and Anderson, D.G. (2015). Optimization of lipid nanoparticle formulations for mRNA delivery in vivo with fractional factorial and definitive screening designs. Nano Lett. *15*, 7300–7306.

53. Fenton, O.S., Kauffman, K.J., McClellan, R.L., Appel, E.A., Dorkin, J.R., Tibbitt, M.W., Heartlein, M.W., DeRosa, F., Langer, R., and Anderson, D.G. (2016). Bioinspired Alkenyl Amino Alcohol Ionizable Lipid Materials for Highly Potent In Vivo mRNA Delivery. Adv. Mater. *28*, 2939–2943.

54. Pardi, N., Tuyishime, S., Muramatsu, H., Kariko, K., Mui, B.L., Tam, Y.K., Madden, T.D., Hope, M.J., and Weissman, D. (2015). Expression kinetics of nucleoside-modified mRNA delivered in lipid nanoparticles to mice by various routes. J. Control. Release *217*, 345–351.

55. Lin, Q., Chen, J., Zhang, Z., and Zheng, G. (2014). Lipid-based nanoparticles in the systemic delivery of siRNA. Nanomedicine (Lond.) *9*, 105–120.

56. Akinc, A., Querbes, W., De, S., Qin, J., Frank-Kamenetsky, M., Jayaprakash, K.N., Jayaraman, M., Rajeev, K.G., Cantley, W.L., Dorkin, J.R., et al. (2010). Targeted delivery of RNAi therapeutics with endogenous and exogenous ligand-based mechanisms. Mol. Ther. *18*, 1357–1364.

57. Zhao, X.B., and Lee, R.J. (2004). Tumor-selective targeted delivery of genes and antisense oligodeoxyribonucleotides via the folate receptor. Adv. Drug Deliv. Rev. *56*, 1193–1204.

58. Li, S.D., Chono, S., and Huang, L. (2008). Efficient gene silencing in metastatic tumor by siRNA formulated in surface-modified nanoparticles. J. Control. Release *126*, 77–84.

59. Chen, C.W., Lu, D.W., Yeh, M.K., Shiau, C.Y., and Chiang, C.H. (2011). Novel RGD-lipid conjugate-modified liposomes for enhancing siRNA delivery in human retinal pigment epithelial cells. Int. J. Nanomedicine *6*, 2567–2580.

60. McCaskill, J., Singhania, R., Burgess, M., Allavena, R., Wu, S., Blumenthal, A., and McMillan, N.A.J. (2013). Efficient Biodistribution and Gene Silencing in the Lung epithelium via Intravenous Liposomal Delivery of siRNA. Mol. Ther. Nucleic Acids *2*, e96.

61. Maruyama, K. (2011). Intracellular targeting delivery of liposomal drugs to solid tumors based on EPR effects. Adv. Drug Deliv. Rev. *63*, 161–169.

62. Love, K.T., Mahon, K.P., Levins, C.G., Whitehead, K.A., Querbes, W., Dorkin, J.R., Qin, J., Cantley, W., Qin, L.L., Racie, T., et al. (2010). Lipid-like materials for low-dose, in vivo gene silencing. Proc. Natl. Acad. Sci. USA *107*, 1864–1869.

63. Ohshima, T., Murray, G.J., Swaim, W.D., Longenecker, G., Quirk, J.M., Cardarelli, C.O., Sugimoto, Y., Pastan, I., Gottesman, M.M., Brady, R.O., and Kulkarni, A.B. (1997). alpha-Galactosidase A deficient mice: a model of Fabry disease. Proc. Natl. Acad. Sci. USA *94*, 2540–2544.

64. Ishii, S., Kase, R., Sakuraba, H., Taya, C., Yonekawa, H., Okumiya, T., Matsuda, Y., Mannen, K., Takeshita, M., and Suzuki, Y. (1998). α-galactosidase transgenic mouse: heterogeneous gene expression and posttranslational glycosylation in tissues. Glycoconj. J. *15*, 591–594.

65. Schiffmann, R., Murray, G.J., Treco, D., Daniel, P., Sellos-Moura, M., Myers, M., Quirk, J.M., Zirzow, G.C., Borowski, M., Loveday, K., et al. (2000). Infusion of α-galactosidase A reduces tissue globotriaosylceramide storage in patients with Fabry disease. Proc. Natl. Acad. Sci. USA *97*, 365–370.

66. Xu, Y., Ou, M., Keough, E., Roberts, J., Koeplinger, K., Lyman, M., Fauty, S., Carlini, E., Stern, M., Zhang, R., et al. (2014). Quantitation of physiological and biochemical barriers to siRNA liver delivery via lipid nanoparticle platform. Mol. Pharm. *11*, 1424–1434.

67. Fechter, P., and Brownlee, G.G. (2005). Recognition of mRNA cap structures by viral and cellular proteins. J. Gen. Virol. *86*, 1239–1249.

YMTHE, Volume *27*

Supplemental Information

Improved Efficacy in a Fabry Disease Model Using a Systemic mRNA Liver Depot System as Compared to Enzyme Replacement Therapy

Frank DeRosa, Lianne Smith, Yinghua Shen, Yan Huang, Jing Pan, Hongsheng Xie, Barak Yahalom, and Michael W. Heartlein

Supporting Information:

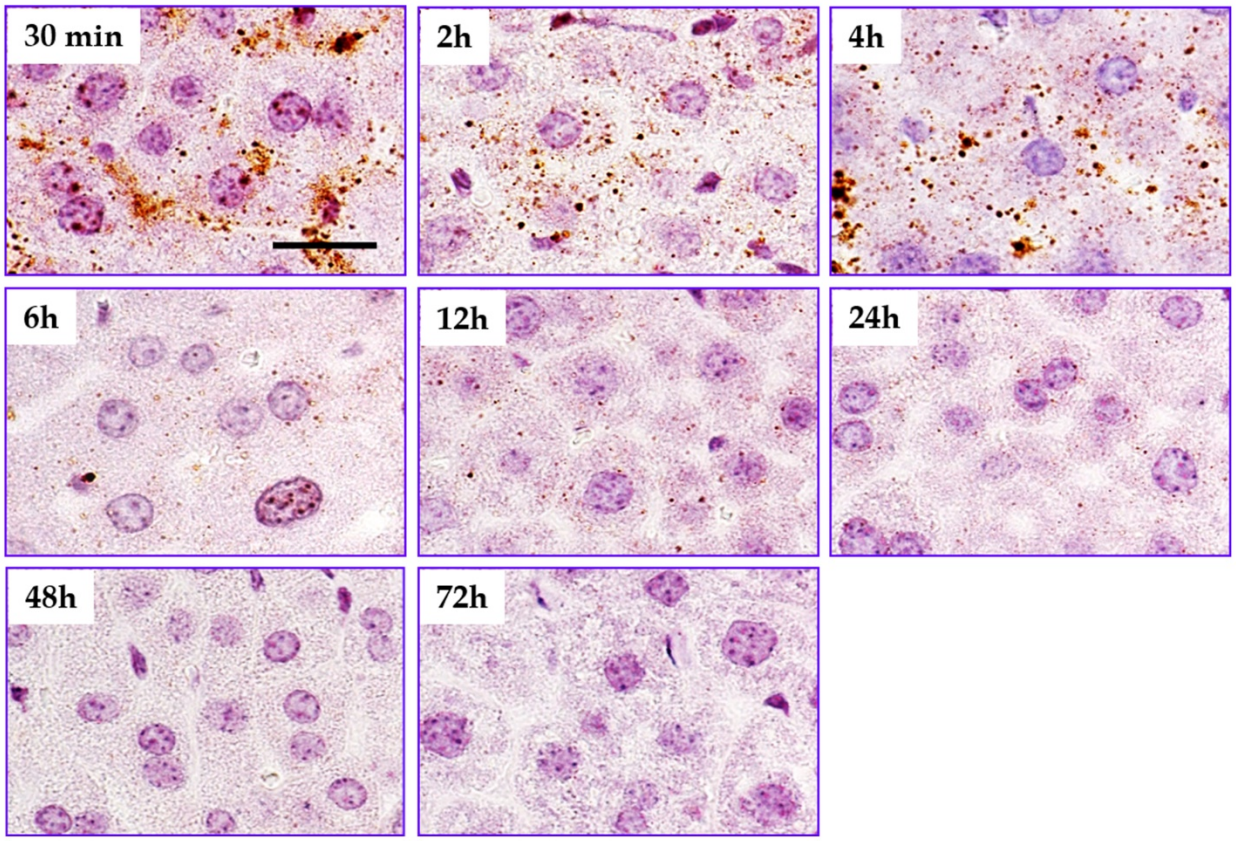

Supplemental Figure 1. Detection of exogenous human GLA mRNA via *in situ* hybridization. Positive staining was observed in hepatocytes as well as sinusoidal cells. Strong detection was observed at the earliest time point (30 minutes) with remnant staining detectable up to 48 hours post-administration of 1.0 mg/kg hGLA mRNA-loaded LNPs. Scale bar = 25 µm.

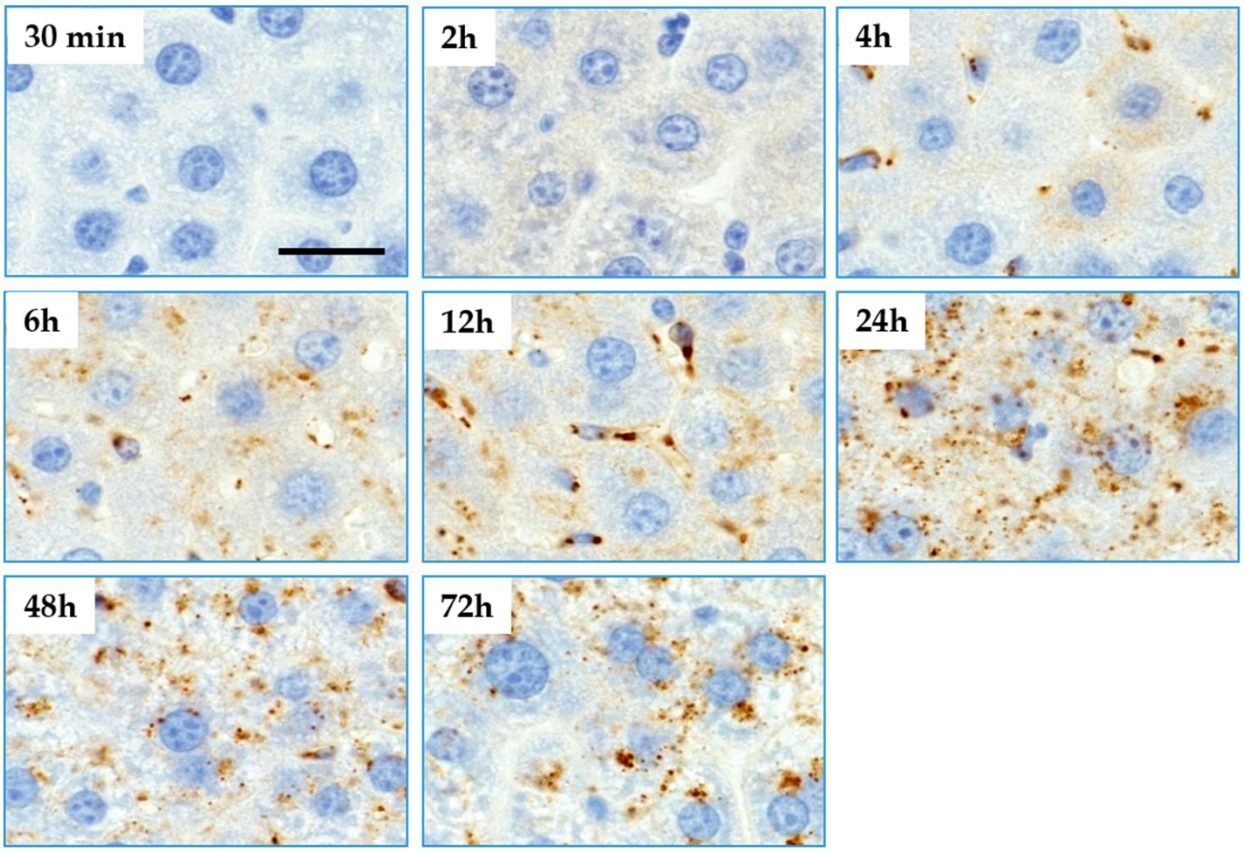

Supplemental Figure 2. Detection of MRT-derived human GLA protein via immunohistochemical staining. Positive staining was observed in hepatocytes as well as sinusoidal cells. Initial visualization is observed as early as two hours post-administration with maximum staining intensity present at 24 hours. Strong detection was observed out to 72 hours. Scale bar = 25 μm

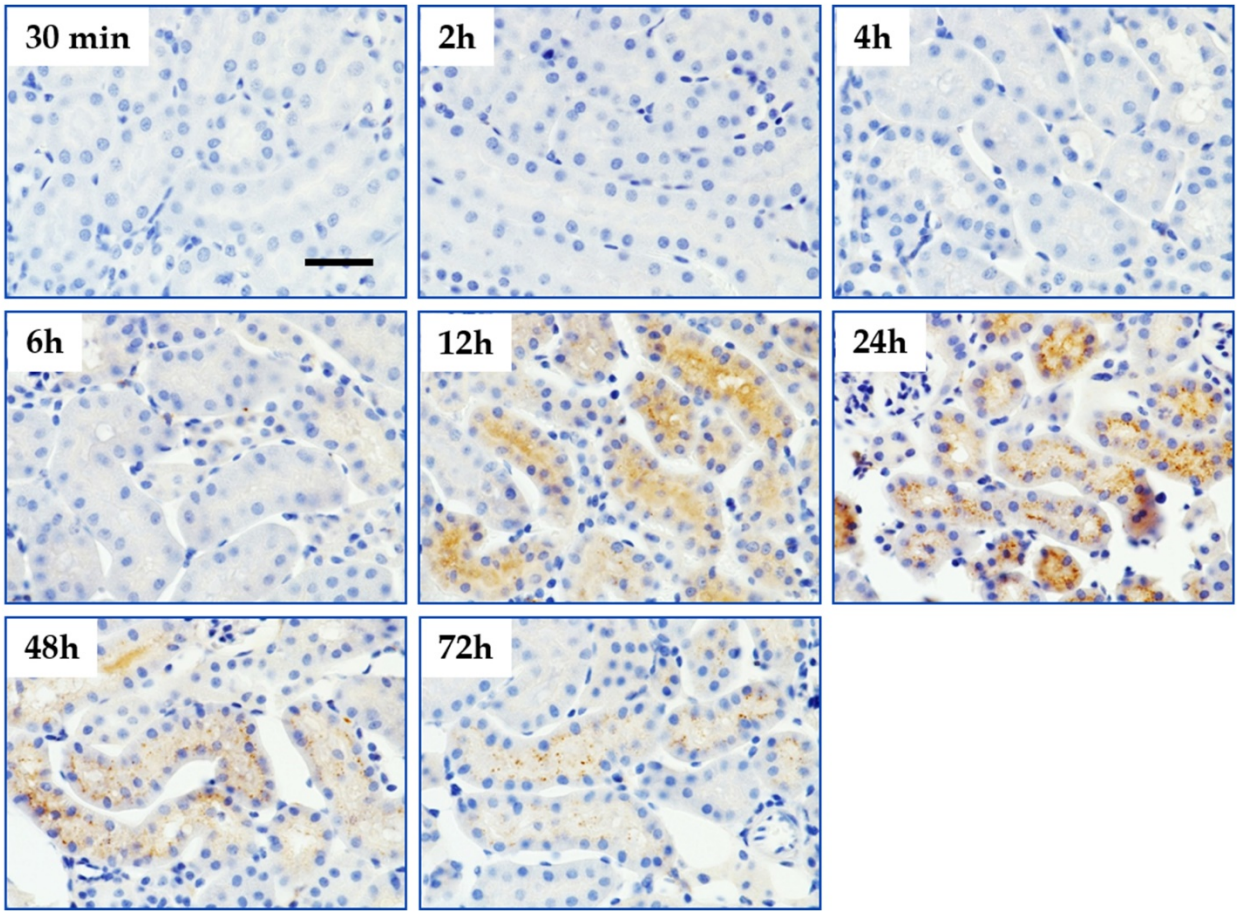

Supplemental Figure 3. Detection of MRT-derived human GLA protein via immunohistochemical staining within the kidneys of wild-type mice post-treatment. Significant detection of hGLA protein was observed predominantly in the lumen 12 hours post-administration. Intracellular hGLA protein levels increase through 48 hours with detectable levels observed out to 72 hours. Scale bar = 50 µm

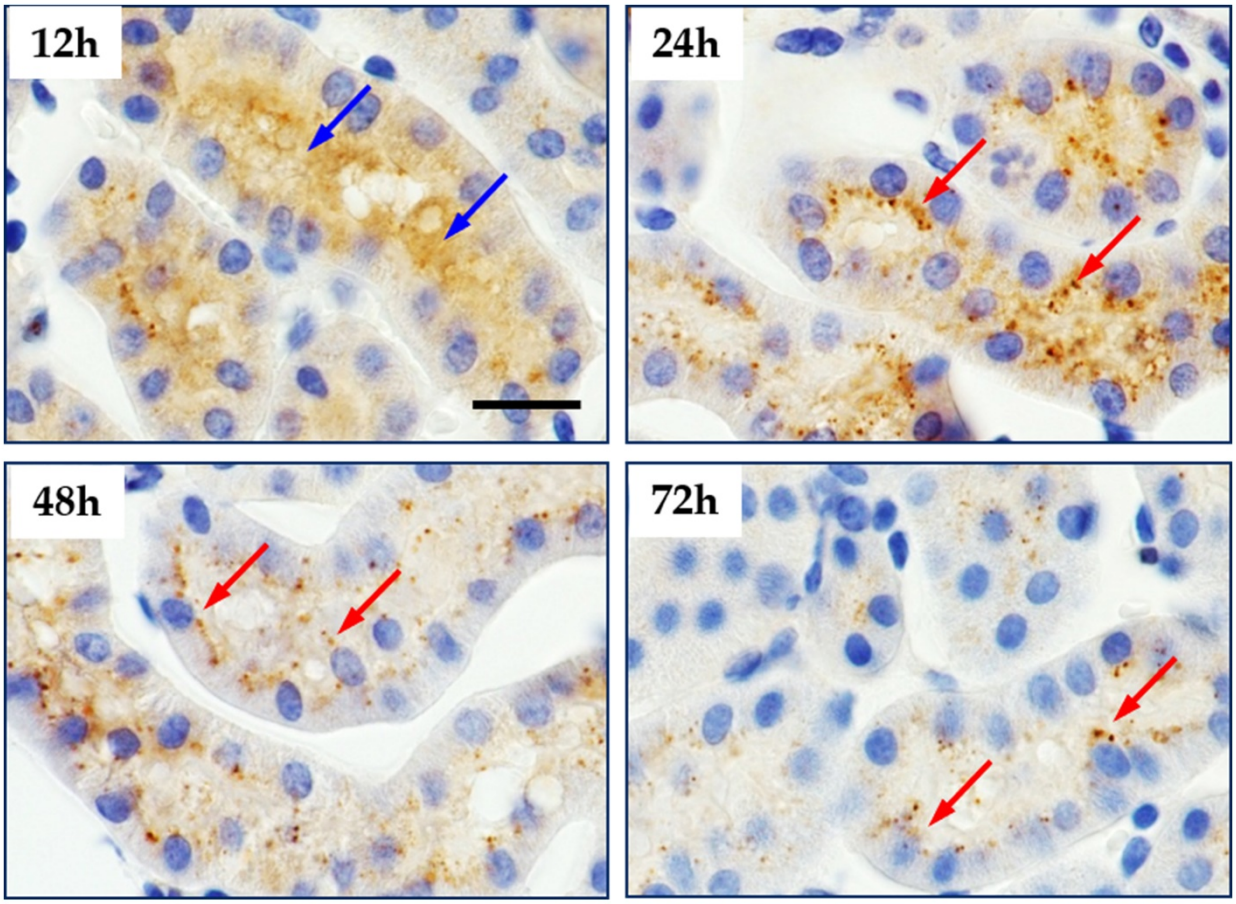

Supplemental Figure 4. Detection of MRT-derived hGLA protein via IHC staining within the kidneys of wild-type mice post-treatment. Significant positive detection of hGLA protein was observed predominantly in the lumen (blue arrows) 12 hours post-administration. More punctate detection of hGLA protein (red arrows) is observed by 24 hours representing an increase in *intracellular* localization. Intracellular levels increase through 48 hours with detectable levels observed out to 72 hours. Scale bar = 25 µm

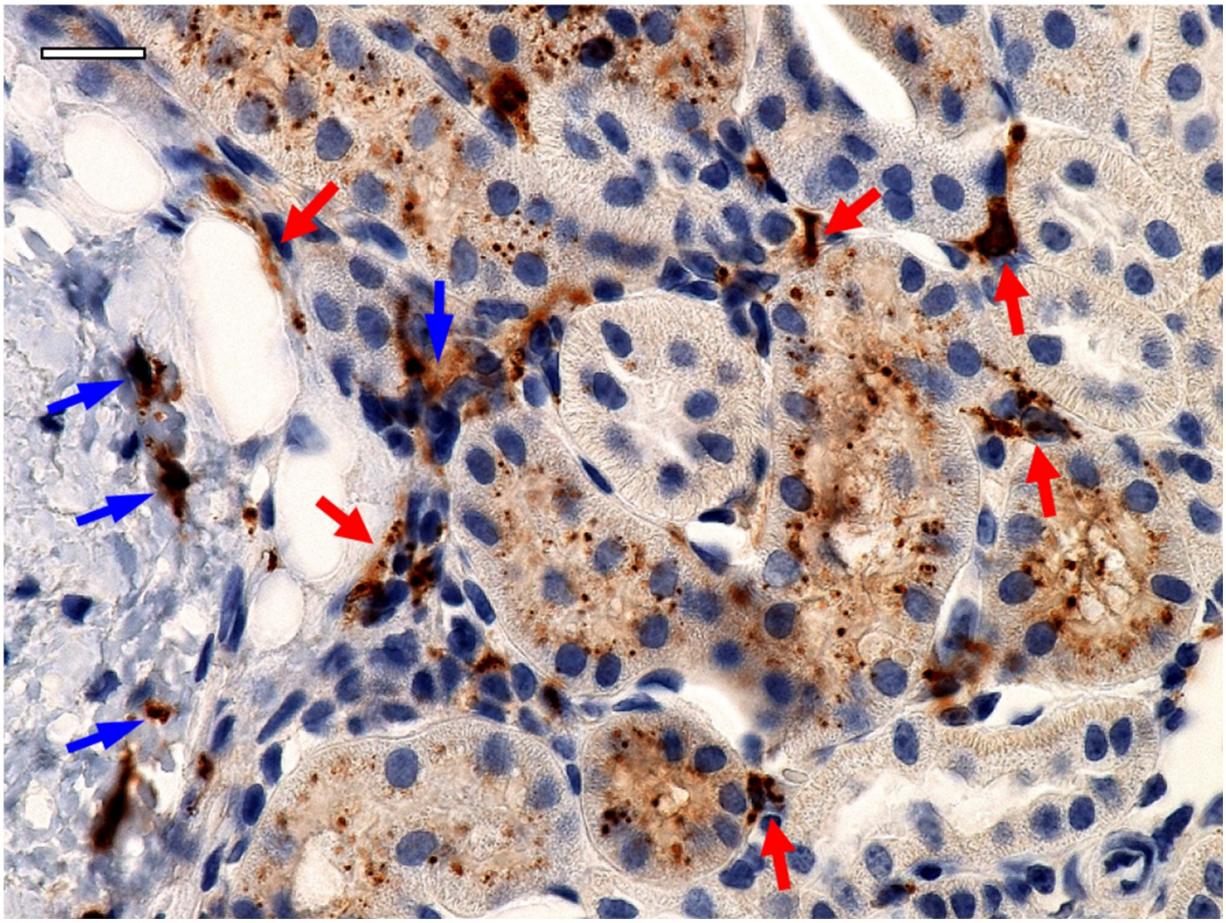

Supplemental Figure 5. High magnification (60x) image using IHC staining demonstrating hGLA cellular uptake within the kidney 24 hours after treatment of hGLA MRT (1.0 mg/kg). Specific detection of hGLA within the interstitial cells (blue arrows) and capillary endothelial cells (red arrows). Scale bar = 25 µm

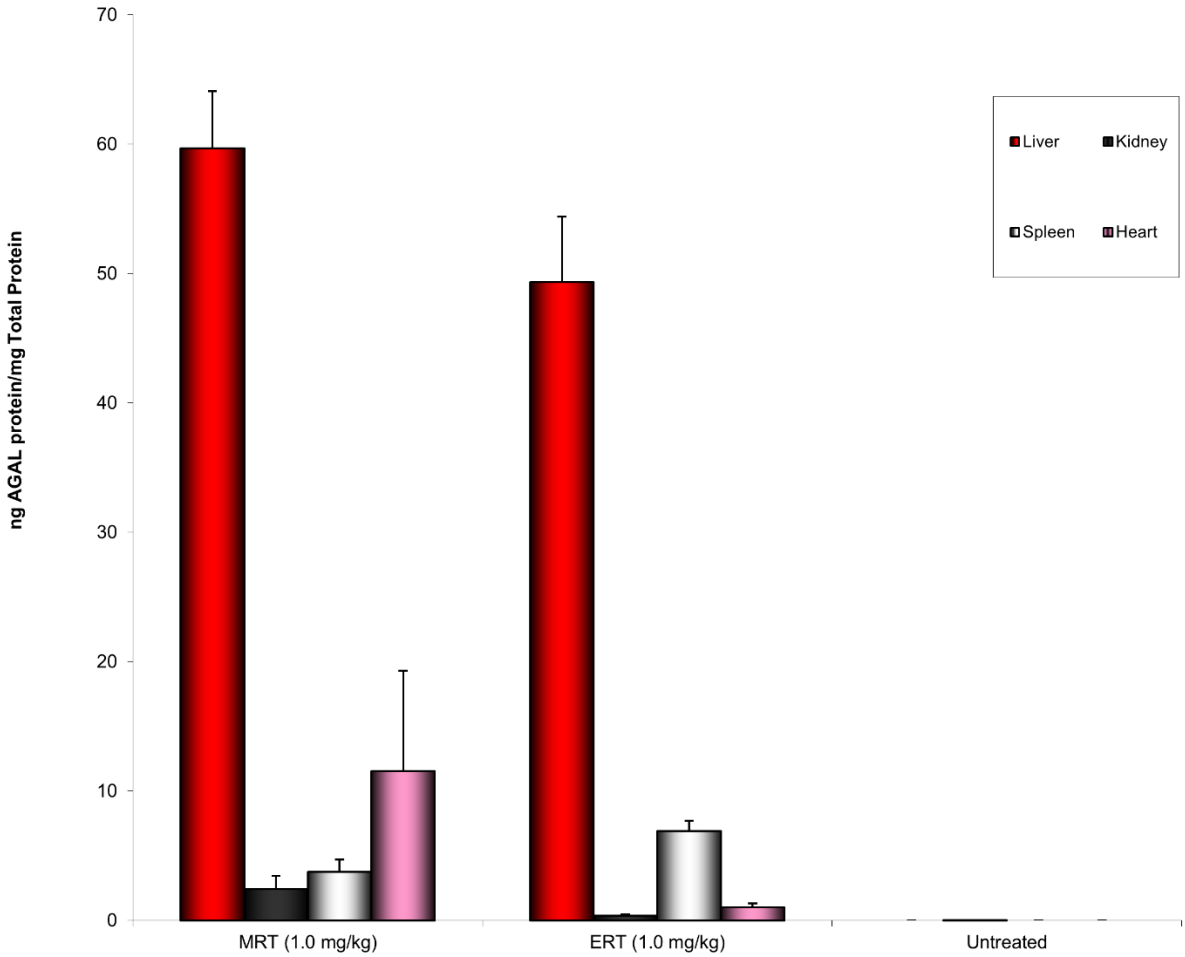

Supplemental Figure 6. Quantification of human α-galactosidase (hGLA) protein levels in selected organs of GLA KO mice one week post-administration of either hGLA MRT or hGLA ERT as measured via ELISA (N=4 mice per group, error bars represent standard deviation). Selected tissues were harvested, homogenized and analyzed. Enhanced hGLA protein accumulation in both the heart and kidneys of hGLA MRT-treated mice was observed as compared to traditional hGLA ERT. Data are means ± SD.

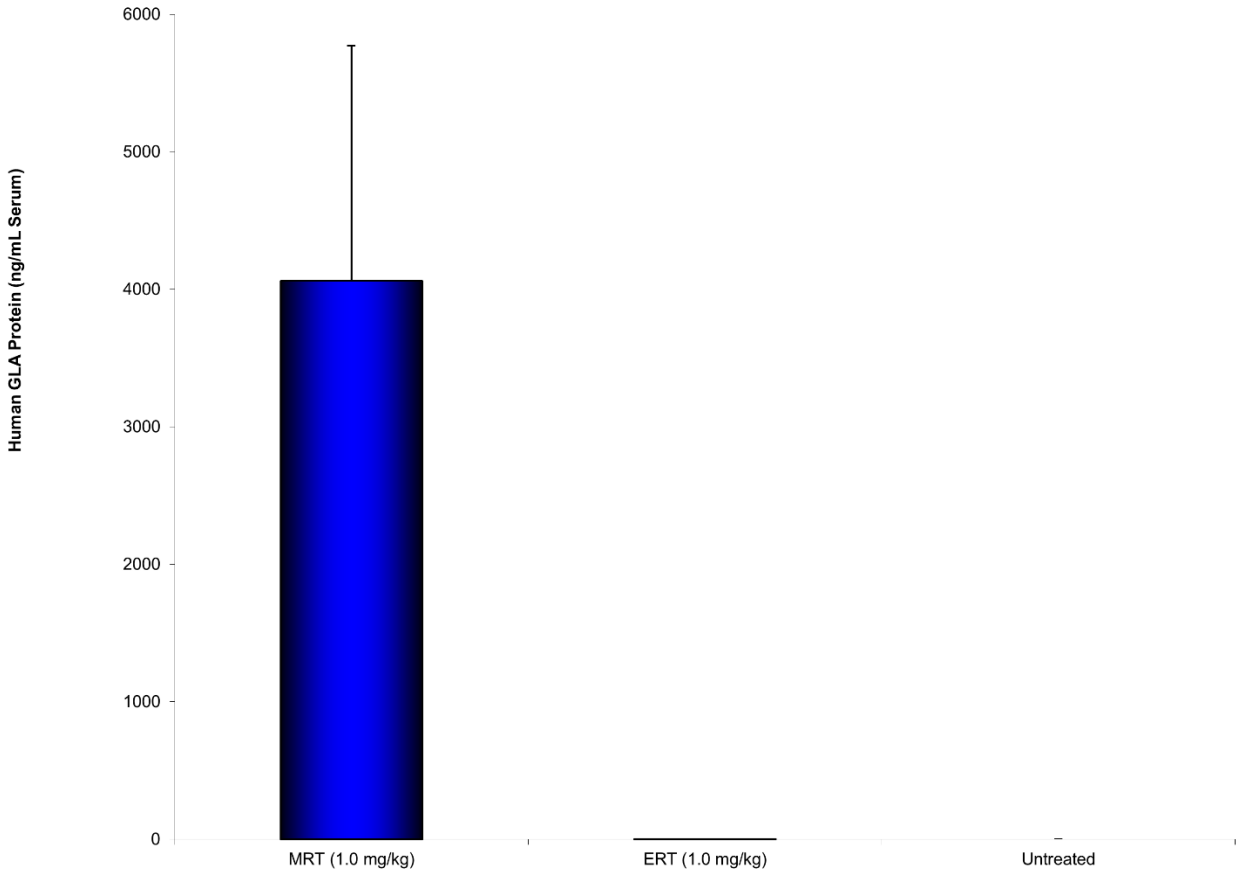

Supplemental Figure 7. Quantification of human α-galactosidase (hGLA) protein levels in GLA KO mice 6 hours post-administration of either hGLA MRT or hGLA ERT as measured via ELISA (N=4 mice per group, error bars represent standard deviation). Detectable serum levels were only achievable after treatment with hGLA MRT. The protein detected is a result of its production from hGLA mRNA delivered intravenously via a single dose of lipid nanoparticles (1.0 mg/kg encapsulated hGLA mRNA). Data are means ± SD.

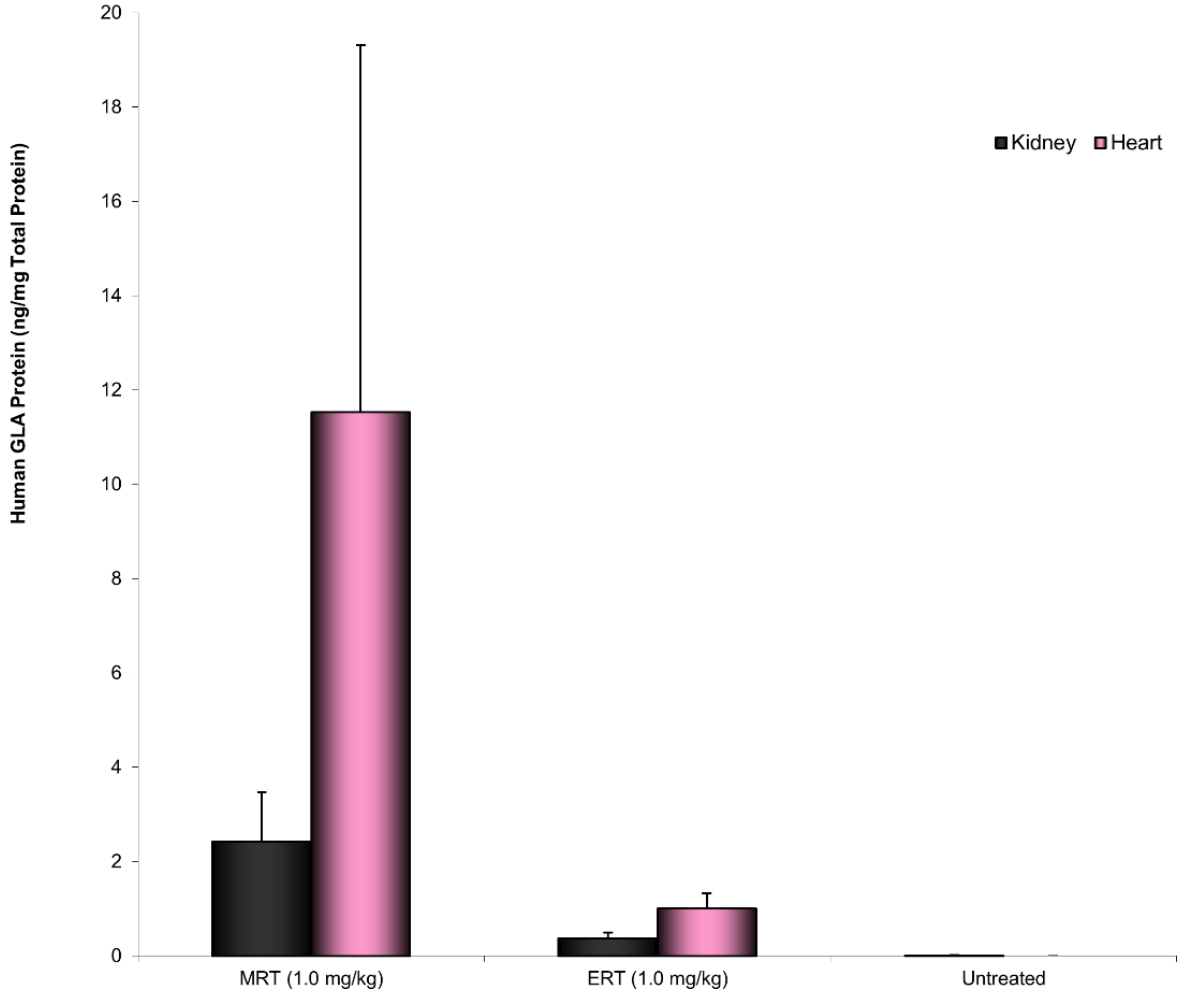

Supplemental Figure 8. Quantification of human α-galactosidase (hGLA) protein levels in selected organs of GLA KO mice one week post-administration of either hGLA MRT or hGLA ERT as measured via ELISA (N=4 mice per group, error bars represent standard deviation). Selected tissues were harvested, homogenized and analyzed. Increased hGLA protein accumulation in both the heart and kidneys of hGLA MRT-treated mice was observed as compared to hGLA ERT. Data are means ± SD.